Journal of Medicinal Chemistry

Article

pubs.acs.org/jmc

Stilbene Boronic Acids Form a Covalent Bond with Human Transthyretin and Inhibit Its Aggregation

Thomas P. Smith,[†,∥,#] Ian W. Windsor,[‡,⊥,∥] Katrina T. Forest,[*,†,§] and Ronald T. Raines[*,†,‡,⊥]

[†]Department of Chemistry, University of Wisconsin—Madison, Madison, Wisconsin 53706, United States
[‡]Department of Biochemistry, University of Wisconsin—Madison, Madison, Wisconsin 53706, United States
[§]Department of Bacteriology, University of Wisconsin—Madison, Madison, Wisconsin 53706, United States

Supporting Information

ABSTRACT: Transthyretin (TTR) is a homotetrameric protein. Its dissociation into monomers leads to the formation of fibrils that underlie human amyloidogenic diseases. The binding of small molecules to the thyroxin-binding sites in TTR stabilizes the homotetramer and attenuates TTR amyloidosis. Herein, we report on boronic acid-substituted stilbenes that limit TTR amyloidosis in vitro. Assays of affinity for TTR and inhibition of its tendency to form fibrils were coupled with X-ray crystallographic analysis of nine TTR·ligand complexes. The ensuing structure−function data led to a symmetrical diboronic acid that forms a boronic ester reversibly with serine 117. This diboronic acid inhibits fibril formation by both wild-type TTR and a common disease-related variant, V30M TTR, as effectively as does tafamidis, a small-molecule drug used to treat TTR-related amyloidosis in the clinic. These findings establish a new modality for covalent inhibition of fibril formation and illuminate a path for future optimization.

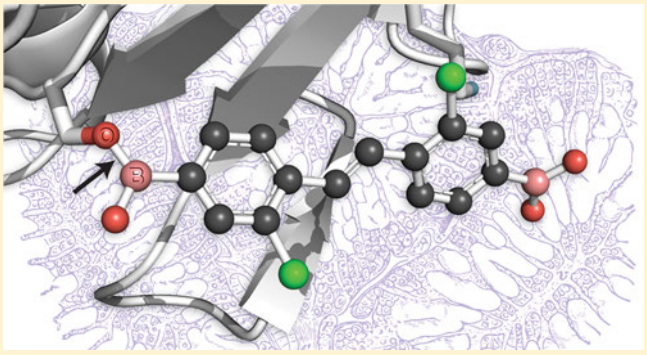

INTRODUCTION

Amyloidosis is a disease caused by the aggregation of a normally soluble protein.[1,2] Endogenous proteins can be causal for these diseases, which include Alzheimer's, Huntington's, and Parkinson's.[3] One such protein, transthyretin (TTR),[4] is a homotetrameric protein composed of four identical monomer units, each consisting of 127 amino acid residues that fold into a β-sandwich (Figure 1).[5,6] The dissociation of the TTR tetramer and aggregation of the ensuing monomers underlies familial amyloid polyneuropathy, familiar cardiomyopathy, and senile systemic amyloidosis.[3,7]

TTR is present in both blood (0.25 g/L = 4 μM) and cerebrospinal fluid (0.1−0.4 μM).[4,8] A primary role of TTR in vivo is to transport thyroxin (T_4) and retinol, a hydrophobic hormone, and fat-soluble vitamin A_1, respectively. Because of the abundance of other lipid-binding proteins (e.g., thyroid-binding globulin and albumin), most of the T_4-binding sites of TTR are empty in blood. In cerebrospinal fluid, TTR also binds to β-amyloid, attenuating the neurotoxicity that underlies Alzheimer's disease.[8−10]

The binding of a ligand can stabilize the folded state of a protein.[11−14] Evidence for the coupling of binding and stability appeared as early as 1890, when O'Sullivan and Thompson demonstrated that cane sugar increases markedly the thermostability of invertase, which is an enzyme that catalyzes the hydrolysis of sucrose.[15] Since then, ligands have been used to enhance the conformational stability of countless proteins, including TTR. Many small molecules have been synthesized and tested as putative TTR ligands, and several have demonstrated efficacy in attenuating amyloidosis.[16,17] Most efforts have focused on ligands that bind to the two identical T_4-binding sites at a dimer−dimer interface (Figure 1), as such ligands discourage dissociation to the monomeric state.[18] A few of these compounds have become viable treatment options, including diflunisal, which is an FDA-approved nonsteroidal anti-inflammatory drug that has had limited adoption due to long-term gastrointestinal side effects associated with cyclooxygenase inhibition,[19,20] and tafamidis, which is used in the clinic to treat TTR-related amyloidosis.[21−23]

An attractive approach to increase the potency and pharmacokinetics of a ligand is to evoke the formation of a covalent bond.[24−26] This strategy is well suited for TTR amyloidosis, not only because with an optimized dosage there might be no appreciable competition in serum with the natural ligand, T_4 but also because sustained stabilization of the TTR tetramer deters the accumulation of monomers that leads to a cascade of aggregation.[27] Previous work by Kelly and coworkers has shown that small molecules can modify TTR chemoselectively by targeting the ε amino group of Lys15/Lys15′ at the entry to the T_4-binding binding site. This work employed irreversible reactions, including conjugate addition

Received: June 28, 2017
Published: September 18, 2017

DOI: 10.1021/acs.jmedchem.7b00952
J. Med. Chem. 2017, 60, 7820−7834

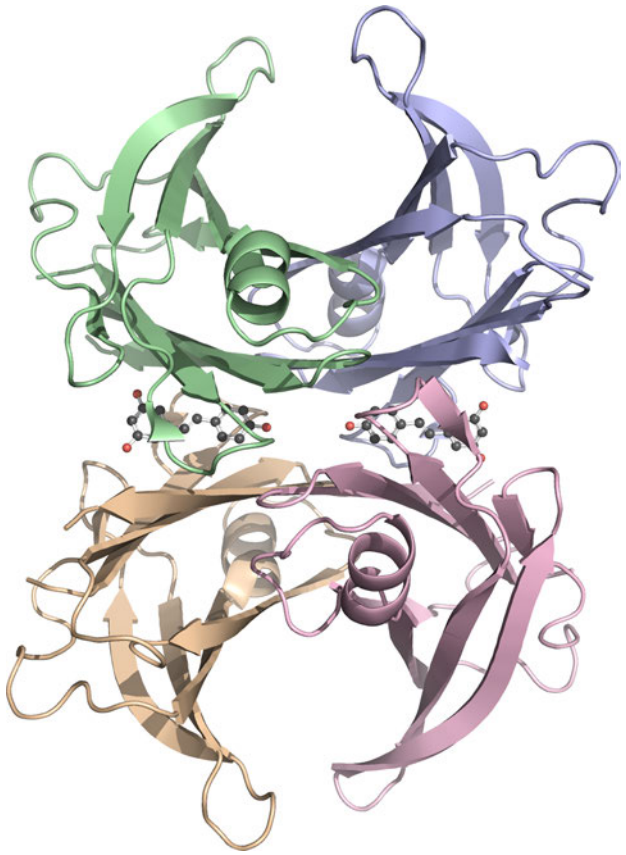

Figure 1. Three-dimensional structure of the TTR·resveratrol complex. TTR monomers (tan, red, green, and purple ribbons) have a β-sandwich fold and assemble into a tetramer, which binds to two molecules of resveratrol (ball-and-stick). The rings of resveratrol (**1**) occupy inner and outer pockets of the two T_4-binding sites at the dimer−dimer interfaces. The image was created with the program PyMOL and PDB entry 1dvs.[5]

with activated esters and thioesters[28,29] and vinyl sulfonamides[30] and sulfation with aryl fluorosulfates.[31,32] Such ligands can, however, react irreversibly with other plasma proteins,[30] leading to potential immunogenic responses to the protein−ligand adduct[24] and the generation of potential toxic byproducts.[29]

To accrue the benefits of covalent binding without the liabilities, we sought ligands for TTR that bind in a *covalent but reversible* manner. Boronic acids interact with Lewis bases in aqueous media.[33,34] Boronic acids (including the FDA-approved drug Bortezomib[35]) are well-known as serine/threonine protease inhibitors,[36−39] antimicrobial and anticancer agents,[40,41] and delivery vehicles.[42−45] Boronic acid-based fluorogenic probes have been developed for sensing both saccharides[46] and reactive oxygen species[47,48] as well as for molecular recognition[49] and protein conjugation.[50,51] These applications arise from the ability of boronic acids to form a covalent bond with a Lewis base that is reversible under physiological conditions.[52,53] Notably, boronic acids are benign, as their metabolic byproduct, boric acid, is present in a normal diet.[54]

Here, we report on the development of boronic acid-based ligands for the T_4-binding site of the TTR tetramer. An iterative strategy involving chemical synthesis and structure−function analysis led us to covalent inhibitors of TTR aggregation. This strategy serves as a model for a new class of amyloidosis inhibitors.

RESULTS

We chose stilbene as a scaffold for the design of an initial series of boronic acid-containing TTR ligands (Chart 1). This scaffold

Chart 1. Diphenol Ligands

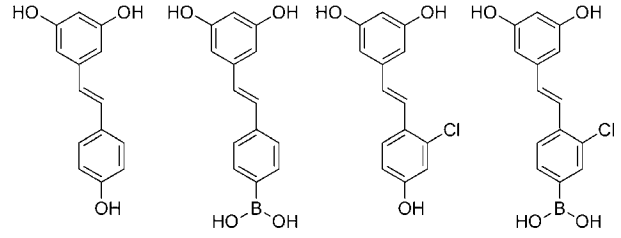

is present in the natural product resveratrol (**1**) and has been employed in other TTR ligands.[5,16,29,55−57] Moreover, stilbenes are readily accessible by a convergent synthetic route, as the two rings can be functionalized separately and then joined with a Wittig reaction (Schemes 1 and 2).

Resveratrol occupies the T_4-binding site with moderate affinity (Table 1 and Figure 1).[5] We began by replacing the phenolic hydroxyl group, which is known to form a hydrogen bond with Ser117/117′ with a boronic acid group to generate stilbene **2** (Chart 1). Halogen substitution is known to provide additional van der Waals interactions within the inner pocket of the T_4-binding site, enhancing the affinity of TTR ligands.[58] Accordingly, we added a chloro group *meta* to the boronic acid moiety to generate stilbenes **3** and **4**.

We performed competitive binding assays to compare affinities among the diphenol series of ligands (Table 1 and Supporting Information, Figure S1A). We observed no change in values of $K_{d,2}$ between stilbene **1** and **2**. Interestingly, chlorinated stilbene **3** showed a higher value of $K_{d,2}$ relative to its nonhalogenated counterpart, stilbene **1**. This decrease in affinity contrasts with stilbene **4**, which exhibited increased affinity as a result of chlorination and showed the strongest affinity for TTR of stilbenes **1**−**4**, having a $K_{d,2}$ value of 441 nM.

Next, we assessed the ability of these molecules to inhibit fibril formation by both wild-type TTR and the common V30M variant, which is associated with familial amyloid polyneuropathy (Table 1 and Supporting Information, Figure S2A). We found that all of the stilbenes in this series inhibited aggregation at 7.2 μM and at a 2:1 ligand/protein ratio. Stilbenes **1** and **2** showed 25% and 23% fibril formation for V30M TTR, whereas stilbenes **3** and **4** showed 14% and 11%, respectively. Herein, we consider compounds that limit aggregation to ≤10% over 96 h as potent inhibitors, and stilbenes **1**−**4** did not achieve this threshold.

Next, we solved co-crystal structures of TTR and resveratrol analogues **2**−**4** to discern if the boronated stilbenes formed a covalent bond with TTR. To our surprise, each phenylboronic acid moiety was observed in the "reverse" binding mode (Figure 2A,B) relative to its parent phenol, resveratrol (Figure 1 and 3A). In other words, the boronic acid group resided in the outer pocket of the T_4-binding site. No indication of boronic ester formation with amino acid residues was apparent (Supporting Information, Figures S4 and S6).

DOI: 10.1021/acs.jmedchem.7b00952
J. Med. Chem. 2017, 60, 7820−7834

Scheme 1. Routes for the Synthesis of Stilbenes 2−6

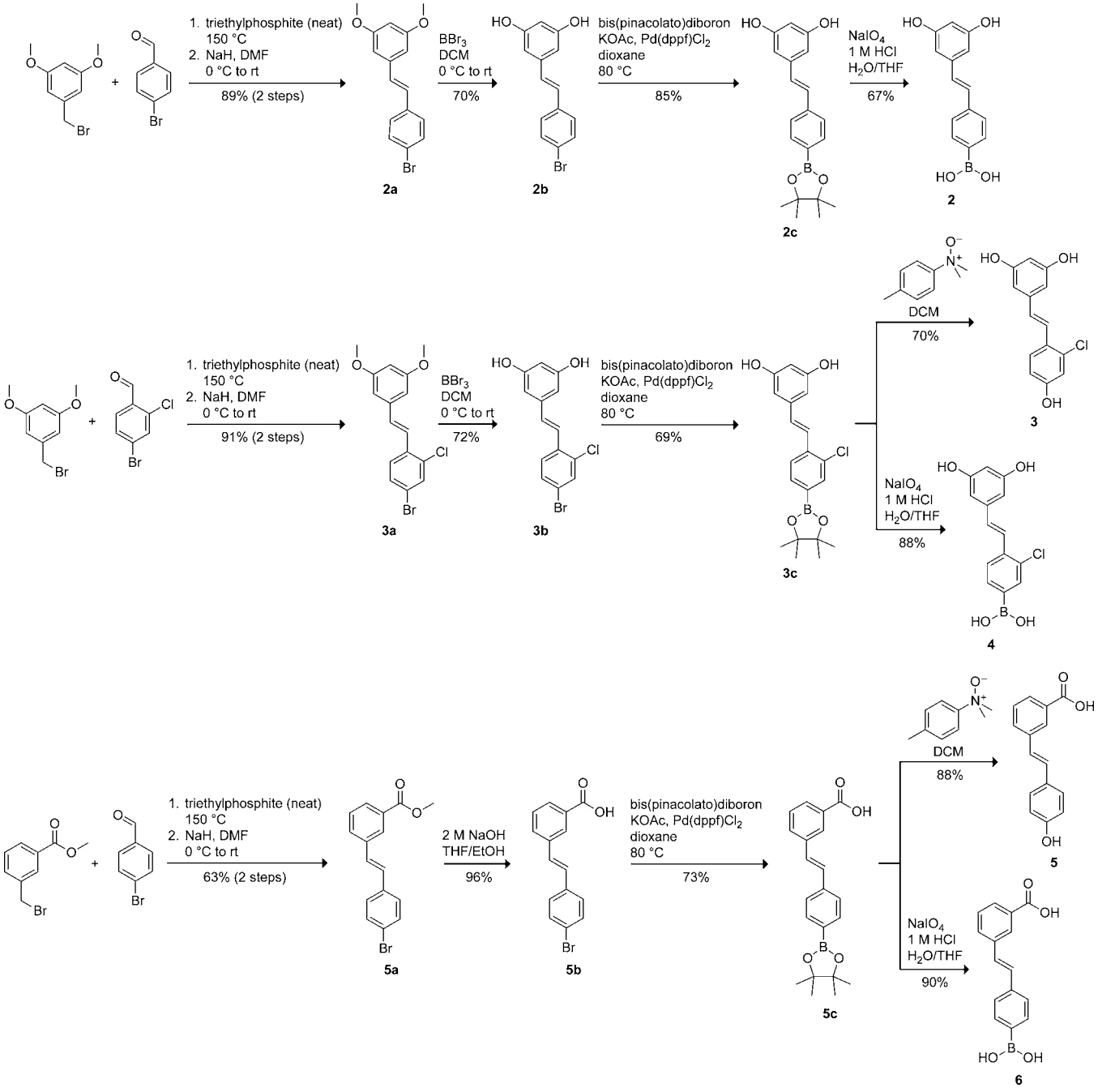

To attempt to reconfigure this unexpected orientation, we designed a second series of stilbenes in which a carboxylic acid group was installed at the *meta* position of the ring not modified in the first series (Chart 2). Previous work had shown that incorporating an anionic substituent into ligands could introduce advantageous electrostatic interactions with Lys15/15′ of TTR.[5,21,59] We hypothesized that this interaction would orient the boronic acid to the inner pocket of the T_4-binding site and perhaps promote boronate−ester formation.

The first pair, stilbenes **5** and **6**, exhibited $K_{d,2}$ values in the low micromolar range, 3- and 2-fold higher than those of stilbenes **1** and **2**, respectively (Table 2 and Supporting Information, Figure S1B). The installation of a chloro group in stilbenes **7** and **8** restored values of $K_{d,2}$ to the high nanomolar range. Consistent with a decreased affinity apparent in the value of $K_{d,2}$, the nonhalogenated stilbenes **5** and **6** also showed a diminished ability to prevent fibril formation under acidic fibril-forming conditions (Table 2 and Supporting Information, Figure S2B). Incubation of wild-type TTR with phenol **5** showed 77% fibril formation and 112% at 7.2 μM for the V30M variant, respectively. Boronic acid **6** performed better as an inhibitor than did phenol **5** for both wild-type TTR and the V30M variant (11% and 28%, respectively). The chlorinated pair **7** and **8** showed potent fibril inhibition (<10%) for both TTRs. These differences were, however, within experimental error. Again, co-crystallography revealed that boronic acids **6** and **8** were bound in the reverse mode, relative to their paired phenols. In other words, the carboxylic acid group was in the

DOI: 10.1021/acs.jmedchem.7b00952
J. Med. Chem. 2017, 60, 7820−7834

Scheme 2. Routes for the Synthesis of Stilbenes 7−11

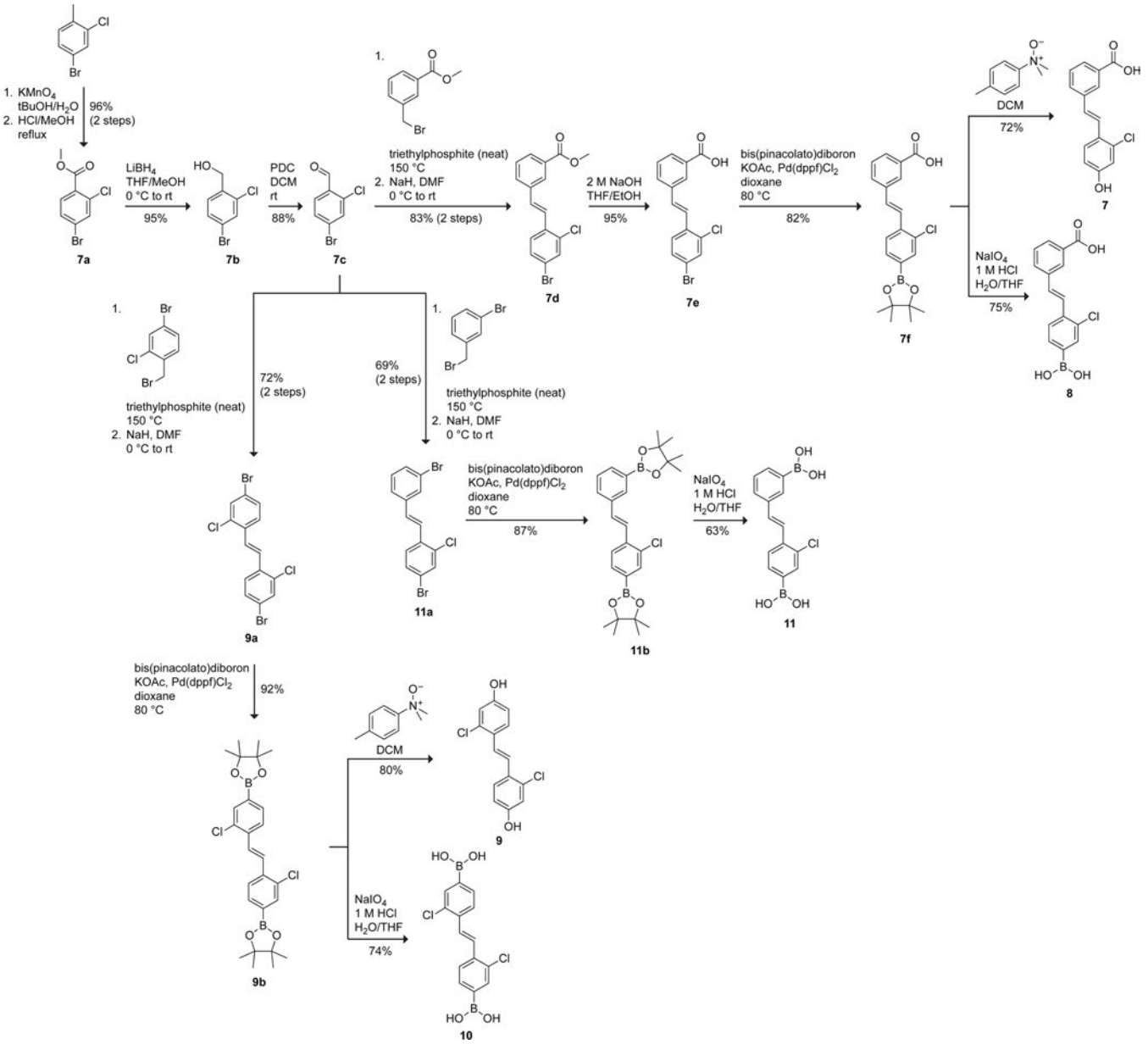

Table 1. Interaction of Diphenols 1−4 with Wild-Type TTR and Its V30M Variant

		wild-type TTR		V30M TTR		
compd	$K_{d,2}$ (μM)	%FF 1:1[a]	%FF 2:1[a]	%FF 1:1[a]	%FF 2:1[a]	binding mode[b]
1 (resveratrol)	0.47 ± 0.03	28 ± 8	9 ± 2	53 ± 12	26 ± 4	forward
2	0.47 ± 0.02	21 ± 4	9 ± 2	48 ± 11	23 ± 6	reverse
3	0.73 ± 0.02	22 ± 4	7 ± 3	44 ± 10	14 ± 4	forward
4	0.44 ± 0.01	19 ± 4	4 ± 2	36 ± 8	12 ± 3	reverse

[a]%FF, percent fibril formation. [b]"forward": upper phenyl ring depicted in Chart 1 lies in the outer pocket of the T_4-binding site, according to X-ray diffraction analysis (Figures 2 and 3). "reverse": upper ring lies in the inner pocket.[18]

inner pocket, near Ser117/117′, and the boronic acid group was in the outer pocket, near Lys15/15′ (Figure 2C,D, and Supporting Information, Table S11). As with boronic acids **2** and **4**, boronic acids **6** and **8** did not exhibit covalent interactions with binding-pocket residues. The structure of **5** in complex with TTR may include alternative conformations for the phenolic group occupying the inner pocket, but we were not confident placing those conformations (Supporting Information, Figures S7A, S7B).

The final series of stilbenes contained a boronic acid moiety on each ring (Chart 3). We synthesized C_2 symmetrical diboronic acid **10**, which has two *meta*-chloro and *para*-boronic acid groups (relative to the stilbene olefin), as well as the analogous C_2 symmetrical diphenol **9**. Additionally, we

DOI: 10.1021/acs.jmedchem.7b00952
J. Med. Chem. 2017, 60, 7820−7834

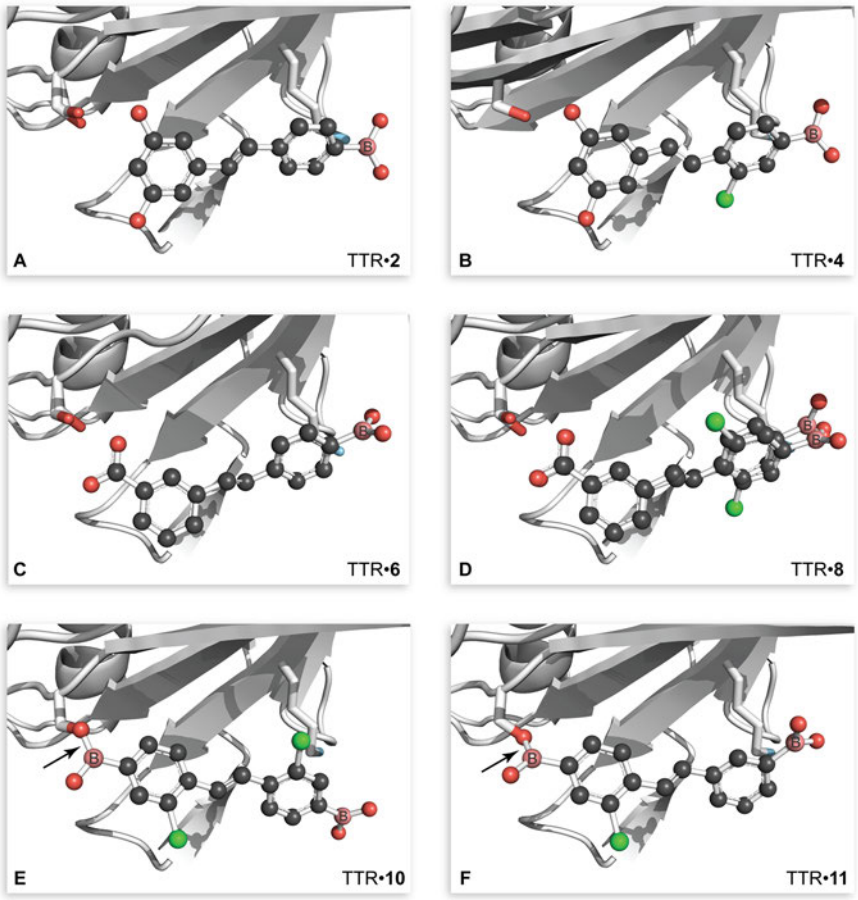

Figure 2. Three-dimensional structures of TTR·ligand complexes that contain a boronic acid group. One monomer (chain B) of the TTR tetramer is shown and is in the same orientation in each panel. The main chain of TTR is rendered as a ribbon, and the side chains of Lys15 and Ser117 are shown explicitly. Ligands are depicted in a ball-and-stick rendition with CPK coloring and boron atoms labeled explicitly. Alternative conformations of Ser117 or the ligand are shown in some panels. Arrows indicate the $O_{117}{}^{\gamma}$–B bond in the TTR·**10** and TTR·**11** complexes. Images were created with the program PyMOL. (A) TTR·**2** (PDB entry 5u48). (B) TTR·**4** (5u4a). (C) TTR·**6** (5u4c). (D) TTR·**8** (5u4e). (E) TTR·**10** (5u4f). (F) TTR·**11** (5u4g).

synthesized stilbene **11**, which has one boronic acid group *meta* to the linker, to investigate whether this position of the boronic acid enhances interactions with Lys15/15′ in the outer pocket. We also included tafamidis (**12**) in this series as a benchmark for our assays.

In the competitive binding assay, diphenol **9** had a $K_{d,2}$ value of 819 nM (Table 3 and Supporting Information, Figure S1C). The analogous diboronic acid, **10**, had a $K_{d,2}$ value of 469 nM, which was the largest decrease in $K_{d,2}$ value that we observed between a boronic acid and its paired phenol. These two stilbenes comprise the only pair that can be compared directly, as their C_2 symmetry precludes alternative binding orientations. The difference in affinity for TTR was amplified in the fibril formation assay, where diboronic acid **10** exhibited more potent inhibition of fibril formation than did diphenol **9**, both for wild-type TTR (3% versus 12% at 7.2 μM) and for the V30M variant (8% versus 27% at 7.2 μM) (Table 1 and Supporting Information, Figure S2C). The binding of diboronic acid **10** with TTR was reversible, as assessed with mass spectrometry (Supporting Information, Figure S3). Asymmetric diboronic acid **11** had a value of $K_{d,2}$ similar to that of diphenol **9** (864 nM) as well as a similar ability to inhibit fibril formation, suggesting that the location of the boronic acid plays a role in optimizing interactions within the binding pocket. Gratifyingly, co-crystallographic data of TTR with either diboronic acid **10** or diboronic acid **11** showed the formation of a boronic ester with Ser117/117′ (Figure 2E,F).

DISCUSSION

We sought a new class of small-molecule ligands for TTR, which is a validated target for pharmacological intervention.[7,21−23] Toward that goal, we investigated the effects of incorporating a boronic acid substituent on the well-known stilbene scaffold, embodied in resveratrol (**1**). The results enabled us to reach two conclusions. First, a boronic acid group can enhance the potency of a TTR ligand. Second, a boronate ester can form with a weakly nucleophilic amino acid residue.

The installation of a boronic acid group tends to increase the affinity of a stilbene for TTR. The value of $K_{d,2}$ for each boronic acid ligand for TTR is lower than (or equivalent to) that of its analogous phenol (Tables 1−3). Moreover, a boronic acid group enhances the ability of a stilbene to deter the formation of TTR fibrils (Tables 1−3). Nonetheless, our structural studies revealed that in each complex between TTR and a stilbene containing a single boronic acid group, that group was in the outer pocket of the T_4-binding site, exposed to solvent (Figure 2A−D, Supporting Information, Figures S4, S6, S8, and S10).

The modest increase in affinity incurred by adding a single boronic acid group could be due to a weak noncovalent

DOI: 10.1021/acs.jmedchem.7b00952
J. Med. Chem. 2017, 60, 7820−7834

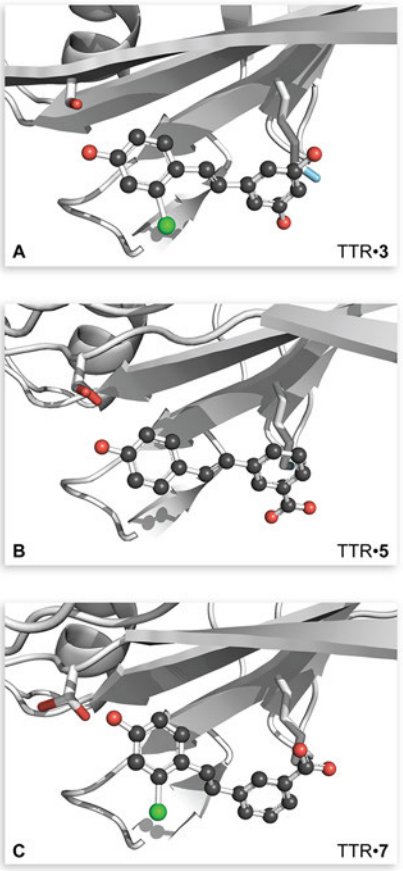

Figure 3. Three-dimensional structures of TTR·ligand complexes that do not contain a boronic acid group. One monomer of the TTR tetramer is shown and is in the same orientation in each panel. The main chain of TTR is rendered as a ribbon, and the side chains of Lys15 and Ser117 are shown explicitly. Ligands are depicted in a ball-and-stick rendition with CPK coloring. Alternative conformations of Ser117 or the ligand are shown in panels B and C. Images were created with the program PyMOL. (A) TTR·**3** (PDB entry 5u49, chain A). (B) TTR·**5** (5u4b, chain B). (C) TTR·**7** (5u4d, chain B).

Chart 2. Carboxylic Acid Ligands

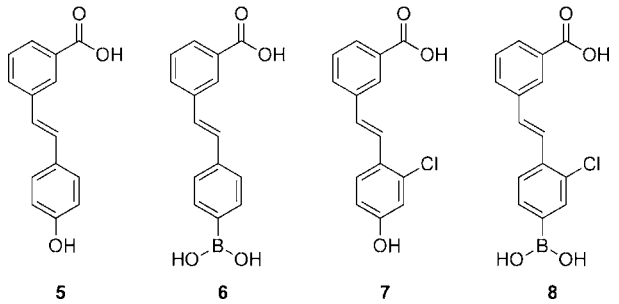

interaction between the ε-amino group of Lys15/15′ and the vacant *p*-orbital of the boron. Kelly and co-workers demonstrated that this amino group, which likely has a low pK_a, can act as a nucleophile.[28] In our complexes, the relevant B···N distances are 3.3−3.5 Å for stilbenes **2**, **4**, **6**, **8**, and **10** (Supporting Information, Table S11). We did not, however, observe electron densities or atomic geometries consistent with the formation of a dative N → B bond between these two functionalities, nor were any additional hydrogen bonds apparent between TTR residues and the boronic acid group (Figure 2A−D, Supporting Information, Figures S4, S6, S8, and S10). Additional hydrogen bonds did, however, arise elsewhere in the complexes with a single boronic acid. For example, the two *meta* hydroxyl groups in stilbenes **2** and **4** (but not **1** and **3**) interact closely (2.0−2.3 Å) with Ser117/117′ (Supporting Information, Table S11).

Stilbenes and similar compounds bind to TTR in one of two modes.[19,27,32,60−63] Although a consensus explanation is not apparent, the polarity of pendant functional groups can play a role in ligand orientation.[56,64] In our stilbenes, however, the relevant log *P* values of phenol (1.46), benzoic acid (1.87), and phenylboronic acid (1.59) are similar,[65] suggesting that hydrophilicity alone contributes little to their orientation in the T_4-binding site. The installation of a chloro group on one ring, as in stilbenes **4** and **8**, led to increased affinity and enhanced efficacy (Tables 1 and 2) but did not affect binding orientation (Figure 2B,D).

To negate binding orientation as a factor, we designed a class of molecules containing a boronic acid substituent on *each* stilbene ring. If such a ligand were to bind to TTR, then a boronic acid group would necessarily be in the inner pocket of the T_4-binding site. We were gratified that this strategy was successful, as the boronic acid group of both stilbenes **10** and **11** that bound in the inner pocket formed an ester with Ser117/117′. Boronic esters have demonstrable utility as mimics of the high-energy tetrahedral intermediate in reactions catalyzed by serine/threonine proteases.[36−39] In those covalent complexes, an active-site serine or threonine residue forms a tetrahedral, sp^3-hybridized boronate ester with a boronic acid group.[66]

Despite the hydration of boronic acid groups in aqueous solution[34] and in marked contrast to other known boronate esters with proteins, we observe planar, sp^2-hybridized boronate esters with Ser117/117′ of TTR (Figure 2E,F). We are aware of only one other structure in which a planar boronate ester is formed with a hydroxyl residue of a protein (PDB entry 1p06).[67] That other structure is, however, distinct because a lone pair of electrons from a proximal histidine residue appears to participate in a dative bond with the vacant *p*-orbital of the boron. The presence of a planar ester could indicate that formation of a tetrahedral adduct is hindered sterically, unlike in the active site of a serine/threonine protease that has evolved to bind tightly to a tetrahedral intermediate. Hence, our results could demarcate the lower limit of affinity enhancement that can be realized from boronic acid-based inhibitors.

Chloro groups have a variable contribution to the affinity of stilbenes for TTR. A chloro group can fill unoccupied cavities, which would otherwise compromise affinity.[68,69] Second, the position of the chloro group in both of the ester-forming boronates enables the formation of a halogen bond.[70] The relevant O···Cl distance is close to the sum of the van der Waals radii ($r_O + r_{Cl}$ = 3.27 Å; Figure 4).[58] The geometries observed in the TTR complexes with stilbenes **10** and **11** (Supporting Information, Table S12) suggest a halogen-bond energy of 0.7−0.9 kcal/mol.[71] Still, the consequences of installing a chloro group on the stilbene scaffold are unlike those of installing a boronic acid group, which consistently increases affinity for TTR (vide supra). For example, the addition of a chloro group to stilbene **1** to form stilbene **3** decreases affinity, whereas the addition of a chloro group to stilbene **5** to form stilbene **7**, increases affinity. Notably, the phenolic ring of stilbene **5** was found to occupy two conformations in the inner pocket of the T_4-binding site, which could explain, in part, the

DOI: 10.1021/acs.jmedchem.7b00952
J. Med. Chem. 2017, 60, 7820−7834

Table 2. Interactions of Carboxylic Acids 5−8 with Wild-Type TTR and its V30M Variant

		wild-type TTR		V30M TTR		
compd	$K_{d,2}$ (μM)	%FF 1:1[a]	%FF 2:1[a]	%FF 1:1[a]	%FF 2:1[a]	binding mode[b]
5	1.8 ± 0.1	75 ± 24	77 ± 14	112 ± 25	120 ± 32	forward
6	0.99 ± 0.02	21 ± 4	11 ± 2	48 ± 12	28 ± 8	reverse
7	0.47 ± 0.01	21 ± 4	3 ± 1	41 ± 10	9 ± 2	forward
8	0.45 ± 0.01	16 ± 4	4 ± 1	32 ± 9	10 ± 2	reverse

[a]%FF, percent fibril formation. [b]"forward": upper phenyl ring depicted in Chart 2 lies in the outer pocket of the T_4-binding site, according to X-ray diffraction analysis (Figures 2 and 3). "reverse": upper ring lies in the inner pocket.[18]

Chart 3. Diboronic Acid and Related Ligands

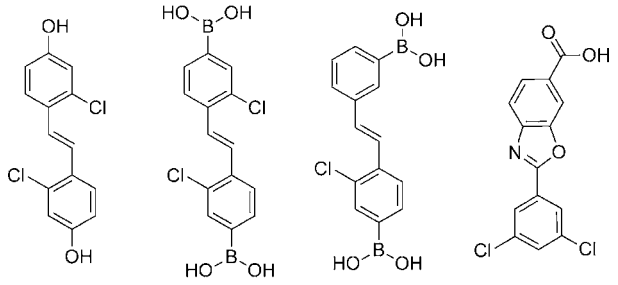

9 **10** **11** **12** (tafamidis)

lower affinity of stilbene **5** relative to stilbene **7** (Figure 3B, Supporting Information, Figures S7, S9).

The judicious use of halogen substituents in boronated stilbenes merits further investigation. For example, a chloro group positioned *meta* to the boron atom has been found to decrease the pK_a of phenyl boronic acid from 8.8 to 8.2.[72] Such a more acidic boronic acid can form more stable boronate esters.[73] An analogous difference in Lewis acidity could be responsible for some of the differences observed in the affinity of boronic acids for TTR.

Likewise, the esterification of TTR by boronic acid ligands warrants additional optimization. In particular, a monoboronate analogue of compound **10** that binds with its lone boronic acid group in the inner pocket could be used to reveal the precise contribution of a boronate ester to the thermodynamics and kinetics[74] of binding. For proper orientation, such a ligand would likely require installation of a highly polar functional group that demands the solvation attainable in the outer pocket.

CONCLUSION

A series of paired stilbenes was designed, synthesized, and tested as ligands for TTR. Each ligand contained either a phenolic hydroxyl group or a phenylboronic acid group, which was intended to bind within the inner pocket of the T_4-binding site in the dimer−dimer interface. We found that the functional groups on the stilbene can alter the binding mode, precluding a rigorous thermodynamic analysis. Nevertheless, our boronic acids are the first ligands observed to form a reversible covalent bond with TTR: one with a serine residue deep in the inner pocket. Crystal structures also revealed the first sp^2-hybridized boronic esters observed with a protein. These stilbene boronic acids inhibit the TTR fibril formation that leads to amyloidosis. Their efficacy extends to V30M TTR, which is a common disease-related variant. We envision that the unique attributes of boronic acid groups could find utility in pharmacological stabilizers of other proteins.

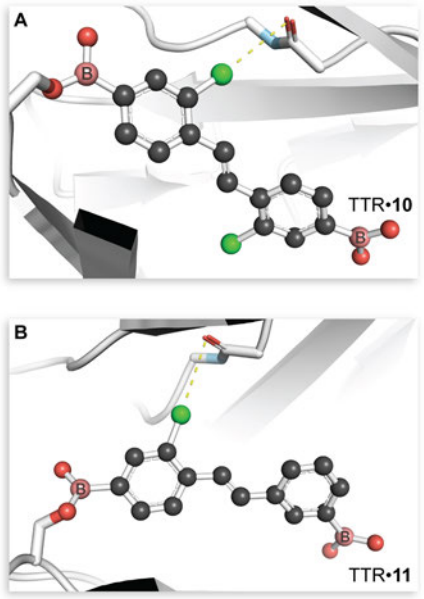

Figure 4. Halogen-bonding interactions in the TTR·**10** and TTR·**11** complexes. One monomer (chain B) of the TTR tetramer is shown. Chloro groups in the two ester-forming boronates exhibit C−Cl··· O_{108}' angles that are nearly linear and Cl··· O_{108}' distances (dashed yellow lines) that are 3.6−3.8 Å (Supporting Information, Table S12). Images were created with the program PyMOL. (A) TTR·**10** (PDB entry 5u4f). (B) TTR·**11** (5u4g).

Table 3. Interactions of Compounds 9−12 with Wild-Type TTR and its V30M Variant

		wild-type TTR		V30M TTR		
compd	$K_{d,2}$ (μM)	%FF 1:1[a]	%FF 2:1[a]	%FF 1:1[a]	%FF 2:1[a]	binding mode[b]
9	0.82 ± 0.01	30 ± 6	12 ± 2	62 ± 16	27 ± 10	ND[c]
10	0.47 ± 0.03	20 ± 3	3 ± 3	32 ± 9	8 ± 3	covalent
11	0.79 ± 0.03	26 ± 4	10 ± 3	54 ± 16	16 ± 5	forward/covalent
12 (tafamidis)	0.37 ± 0.01	22 ± 5	0 ± 6	5 ± 13	8 ± 7	forward[d]

[a]%FF, percent fibril formation. [b]"forward": upper phenyl ring depicted in Chart 3 lies in the outer pocket of the T_4-binding site, according to X-ray diffraction analysis (Figure 2).[18] "covalent": formation of a boronate ester with Ser117. [c]ND, not determined. [d]Reference 21.

DOI: 10.1021/acs.jmedchem.7b00952
J. Med. Chem. 2017, 60, 7820−7834

EXPERIMENTAL SECTION

Materials. Resveratrol (**1**), 8-anilino-1-naphthalenesulfonic acid (ANS), and other reagents for biochemical assays were from Sigma–Aldrich (St. Louis, MO). Tafamidis (2-(3,5-dichlorophenyl)-6-benzoxazolecarboxylic acid) (**12**) was from Carbosynth Limited (Berkshire, UK). DNA oligonucleotides were from Integrated DNA Technologies (Coralville, IA).

Chemical Synthesis. Stilbenes **2**–**11** were synthesized by the routes shown in Schemes 1 and 2.

Materials. Reagents and solvents were from Sigma–Aldrich (Milwaukee, WI) and were used without further purification. All glassware was flame-dried, and all reactions were performed under an atmosphere of N_2(g). Reagent-grade solvents: dichloromethane (DCM), tetrahydrofuran (THF), triethylamine (TEA), and dimethylformamide (DMF) were dried over a column of alumina and were removed from a dry still under an inert atmosphere. Flash column chromatography was performed with Silicycle 40–63 Å silica (230–400 mesh), and thin-layer chromatography (TLC) was performed with EMD 250 μm silica gel 60 F_{254} plates.

Conditions. All procedures were performed in air at ambient temperature (~22 °C) and pressure (1.0 atm) unless indicated otherwise.

Solvent Removal. The phrase "concentrated under reduced pressure" refers to the removal of solvents and other volatile materials using a rotary evaporator at water aspirator pressure (<20 Torr) while maintaining a water bath below 40 °C. Residual solvent was removed from samples at high vacuum (<0.1 Torr).

NMR Spectroscopy. ^{1}H and ^{13}C NMR spectra were acquired with a Bruker Avance III 500i spectrometer at the National Magnetic Resonance Facility at Madison (NMRFAM). Chemical shift data are reported in units of δ (ppm) relative to residual solvent.

Mass Spectrometry. Mass spectra of small molecules were acquired with an LCT electrospray ionization (ESI) instrument from Waters. Mass spectra of proteins were acquired with a microflex LRF desorption ionization–time-of-flight (MALDI–TOF) instrument from Bruker (Billerica, MA). Both instruments were in the Paul Bender Chemical Instrumentation Center at the University of Wisconsin—Madison.

Melting Points. Melting points were determined with an OptiMelt MPA100 instrument from Stanford Research Systems (Sunnyvale, CA) over a range of 100–400 °C with a 0.5 °C/min heating rate. Melting points values are given as the single meniscus point. Compounds **2**, **3**, and **5** had melting points >400 °C.

Compound Purity. The purity of all compounds was judged to be ≥95%, as assessed by ^{1}H and ^{13}C NMR spectroscopy, mass spectrometry, melting-point determination, and reversed-phase high-performance liquid chromatography (HPLC) using a C18 column and 515/717/996 analytical instrument from Waters (Milford, MA) with a gradient of 10–80% v/v acetonitrile in water over 40 min.

*5-[(1E)-2-(4-Bromo)ethenyl]-1,3-dimethoxybenzene (**2a**).* 3,5-Dimethoxybenzyl bromide (1.2 g, 5.5 mmol) was dissolved in neat triethylphosphite (1.2 mL, 6.6 mmol) and heated to 150 °C for 4 h. The reaction mixture was cooled to 0 °C and diluted with DMF (40 mL). NaH (60% w/v in mineral oil, 0.28 g, 7.12 mmol) was added to the resulting solution, and the reaction mixture was stirred at 0 °C for 20 min. A solution of 4-bromo-benzaldehyde (1.0 g, 5.5 mmol) in DMF (15 mL) was then added dropwise. The reaction mixture was allowed to warm to room temperature and stirred overnight. The reaction mixture was then diluted with EtOAc (20 mL) and washed with 10% w/v citric acid (30 mL), followed by brine (30 mL). The organic layer was separated, dried with Na_2SO_4(s), and filtered. The solvent was removed under reduced pressure, and the crude product was purified by flash column chromatography (10% v/v EtOAc in hexanes) to afford compound **2a** as a white solid (1.56 g, 89%). ^{1}H NMR (500 MHz, $CDCl_3$, δ): 3.83 (s, 6H), 6.41 (s, 1H), 6.65 (s, 2H), 6.98–7.01 (d, J = 16.28 Hz, 1H), 7.01–7.04 (d, J = 16.34 Hz, 1H), 7.35–7.37 (d, J = 8.48 Hz, 2H), 7.46–7.48 (d, J = 8.51 Hz, 2H). ^{13}C NMR (100 MHz, $CDCl_3$, δ): 55.42, 100.31, 104.74, 121.57, 128.03, 128.16, 129.50, 131.92, 136.19, 139.07, 161.12. ASAP–MS (m/z): [M + H]$^+$ calcd for $C_{16}H_{15}BrO_2$, 319.0329; found, 319.0331.

*5-[(1E)-2-(4-Bromo)ethenyl]-1,3-benzenediol (**2b**).* Compound **2a** (0.5 g, 1.6 mmol) was dissolved in DCM (7 mL), and the resulting solution was cooled to 0 °C. A solution of 1.0 M BBr_3 in DCM (7.8 mL) was added dropwise at 0 °C. The reaction mixture was allowed to warm to room temperature and stirred for 4 h. The reaction mixture was then poured carefully into a separation funnel containing ice–water (~15 mL). The mixture was extracted with DCM (3 × 15 mL). The organic layers were combined and washed with brine (15 mL), dried with Na_2SO_4(s), and filtered. The solvent was removed under reduced pressure, and the crude product was suspended in ice-cold DCM. The resulting precipitate was isolated by filtration to afford compound **2b** as a white solid (0.326 g, 70%). ^{1}H NMR (500 MHz, CD_3OD, δ): 6.22 (s, 1H), 6.51 (s, 2H), 7.00–7.03 (d, J = 16.33 Hz, 1H), 7.04–7.07 (d, J = 16.33 Hz, 1H), 7.45–7.47 (d, J = 8.5 Hz, 2H), 7.50–7.51 (d, J = 8.5 Hz, 2H). ^{13}C NMR (125 MHz, CD_3OD, δ): 103.43, 106.15, 121.97, 128.05, 129.17, 130.97, 132.78, 138.04, 140.42, 159.80. HRMS–ESI (m/z): [M − H]$^-$ calcd for $C_{14}H_{11}BrO_2$, 288.9870; found, 288.9869.

*5-[(1E)-2-(4-Boronic acid pinacol ester)ethenyl]-1,3-benzenediol (**2c**).* Compound **2b** (0.250 g, 0.858 mmol), KOAc (0.245 g, 2.57 mmol), bis(pinacolato)diboron (0.652 g, 2.57 mmol), and Pd(dppf)-Cl_2 (0.062 g, 0.0858 mmol) were added to a Schlenk flask, which was then evacuated and backfilled with N_2(g). Dioxane (8.5 mL) was deoxygenated by sonication under high vacuum and backfilled with N_2(g). The deoxygenated dioxane was then added by cannula into the reaction flask, and the reaction mixture was heated to 80 °C and stirred overnight. The reaction mixture was then filtered, and the solvent was removed under reduced pressure. The crude product was purified by flash column chromatography (20% v/v EtOAc in hexanes) to afford compound **2c** as a white solid (0.245 g, 85%). ^{1}H NMR (500 MHz, CD_3OD, δ): 1.34 (s, 12H), 6.22 (s, 1H), 6.51 (s, 2H), 7.02–7.06 (d, J = 16.27 Hz, 1H), 7.06–7.10 (d, J = 16.36 Hz, 1H), 7.50–7.52 (d, J = 7.93 Hz, 2H), 7.71–7.72 (d, J = 7.79 Hz, 2H). ^{13}C NMR (125 MHz, CD_3OD, δ): 25.19, 85.04, 103.42, 160.21, 126.77, 129.23, 131.16, 136.08, 140.54, 141.63, 159.75. HRMS–ESI (m/z): [M − H]$^+$ calcd for $C_{20}H_{23}BO_4$, 336.1653; found, 336.1653.

*5-[(1E)-2-(4-Boronic acid)ethenyl]-1,3-benzenediol (**2**).* Compound **2c** (0.050 g, 0.147 mmol) was dissolved in 4:1 THF/H_2O (1.5 mL). $NaIO_4$ (0.157 g, 0.739 mmol) was added to the resulting solution, followed by 1.0 M HCl (36 μL, 0.036 mmol). The reaction mixture was allowed to stir overnight. The reaction mixture was then diluted with H_2O (2 mL) and extracted with EtOAc (3 × 4 mL). The organic layers were combined and washed with brine (10 mL), dried with Na_2SO_4(s), and filtered. The solvent was removed under reduced pressure, and the crude product was purified by flash column chromatography (3% v/v CH_3OH in DCM) to afford compound **2** as a white crystalline solid (0.027 g, 67%) with mp >400 °C. ^{1}H NMR (500 MHz, CD_3OD, δ): 6.20 (s, 1H), 6.50 (s, 2H), 7.95 (bs, 2H), 7.51–7.52 (d, J = 8.17 Hz, 2H), 7.60–7.62 (d, J = 8.13 Hz, 2H). ^{13}C NMR (125 MHz, CD_3OD, δ): 103.32, 106.13, 126.69, 129.26, 130.67, 135.09, 140.06, 140.64, 159.78. HRMS–ESI (m/z): [M − H]$^-$ calcd for the single methyl boronic ester $C_{15}H_{15}BO_4$, 268.1027; found, 268.1027.

*5-[(1E)-2-(2-Chloro-4-bromo)ethenyl]-1,3-dimethoxybenzene (**3a**).* 3,5-Dimethoxybenzyl bromide (0.74 g, 3.4 mmol) was dissolved in neat triethylphosphite (0.7 mL, 4.0 mmol), and the resulting solution was heated to 150 °C for 4 h. The reaction mixture was cooled to 0 °C and added to DMF (20 mL). NaH (60% w/v in mineral oil, 0.17 g, 4.36 mmol) was added to the resulting solution, and the reaction mixture was stirred at 0 °C for 20 min. A solution of 4-bromo-2-chloro benzaldehyde (0.74 g, 3.36 mmol) in DMF (10 mL) was then added dropwise. The reaction mixture was allowed to warm to room temperature and stirred overnight. The reaction mixture was then diluted with EtOAc (15 mL) and washed with 10% w/v citric acid (20 mL), followed by brine (20 mL). The organic layer was separated, dried with Na_2SO_4(s), and filtered. The solvent was removed under reduced pressure, and the crude product was purified by flash column chromatography (5% v/v EtOAc in hexanes) to afford

DOI: 10.1021/acs.jmedchem.7b00952
J. Med. Chem. 2017, 60, 7820–7834

compound **3a** as a white solid (1.10 g, 91% over 2 steps). ^{1}H NMR (400 MHz, $CDCl_3$, δ): 3.84 (s, 6H), 6.44 (s, 1H), 6.69 (s, 2H), 6.97−7.01 (d, J = 16.24 Hz, 1H), 7.36−7.40 (m, 2H), 7.50−7.52 (d, J = 8.42 Hz, 1H), 7.55 (s, 1H). ^{13}C NMR (100 MHz, $CDCl_3$, δ): 55.51, 100.60, 105.11, 121.37, 124.27, 127.60, 130.27, 131.89, 132.43, 134.20, 134.41, 138.81, 161.12. ASAP−MS (m/z): $[M + H]^+$ calcd for $C_{16}H_{14}BrClO_2$, 352.9939; found, 352.9939.

*5-[(1E)-2-(2-Chloro-4-bromo)ethenyl]-1,3-benzenediol (**3b**).* Compound **3a** (0.500 g, 1.42 mmol) was dissolved in DCM (14 mL), and the reaction mixture was cooled to 0 °C. A solution of 1.0 M BBr_3 (7.10 mmol) in DCM (7.1 mL) was then added dropwise at 0 °C. The reaction mixture was allowed to warm to room temperature and stirred for 4 h. The reaction mixture was then poured carefully into a separation funnel containing ice−water (∼10 mL) and extracted with DCM (3 × 10 mL). The organic layers were combined and washed with brine (15 mL), dried with Na_2SO_4(s), and filtered. The solvent was removed under reduced pressure, and the crude product was suspended in cold DCM (5 mL). The resulting precipitate was filtered to afford compound **3b** as a white solid (0.335 g, 72%). ^{1}H NMR (500 MHz, CD_3OD, δ): 6.23, (s, 1H), 6.51 (s, 2H), 7.03−7.07 (d, J = 16.23 Hz, 1H), 7.31−7.35 (d, J = 16.23 Hz, 1H), 7.45−7.47 (d, J = 8.31 Hz, 1H), 7.60 (s, 1H), 7.67−7.69 (d, J = 8.47 Hz, 1H). ^{13}C NMR (125 MHz, CD_3OD, δ): 103.79, 106.34, 124.89, 126.71, 133.26, 133.34, 133.90, 135.91, 137.59, 140.29, 159.89. HRMS−ESI (m/z): $[M - H]^-$ calcd for $C_{14}H_{10}BrClO_2$, 322.9480; found, 322.9480.

*5-[(1E)-2-(2-Chloro-4-boronic acid pinacol ester)ethenyl]-1,3-benzenediol (**3c**).* Compound **3b** (0.100 g, 0.308 mmol), KOAc (0.088 g, 0.926 mmol), bis(pinacolato)diboron (0.235 g, 0.926 mmol), and Pd(dppf)Cl_2 (0.0225 g, 0.0308 mmol) were added to a flame-dried Schlenk flask, which was then evacuated and backfilled with N_2(g). Dioxane (3.5 mL) was deoxygenated by sonication under high vacuum and backfilled with N_2(g). The deoxygenated dioxane was then added by cannula into the reaction flask, and the reaction mixture was heated to 80 °C and stirred overnight. The reaction mixture was filtered, and the solvent was removed under reduced pressure. The crude product was purified by flash column chromatography (2% v/v CH_3OH in DCM) to afford compound **3c** as a white solid (0.080 g, 69%). ^{1}H NMR (500 MHz, CD_3OD, δ): 1.33 (s, 12H), 6.23 (s, 1H), 6.53 (s, 2H), 7.05−7.09 (d, J = 16.29 Hz, 1H), 7.40−7.44 (d, J = 16.28 Hz, 1H), 7.60−7.62 (d, J = 7.98 Hz, 1H), 7.70 (s, 1H), 7.72−7.74 (d, J = 7.83 Hz, 1H). ^{13}C NMR (125 MHz, CD_3OD, δ): 25.18, 75.82, 85.42, 103.90, 106.42, 124.82, 126.88, 133.83, 133.90, 134.11, 136.74, 139.11, 140.17, 159.84. HRMS−ESI (m/z): $[M - H]^-$ calcd for $C_{20}H_{22}BClO_4$, 370.1263; found, 370.1263.

*5-[(1E)-2-(2-Chloro-4-hydroxyphenyl)ethenyl]-1,3-benzenediol (**3**).* Compound **3** was derived from the oxidation of compound **3c** by an aryl *N*-oxide in one step as described previously.[75] Here, compound **3c** (0.020 g, 0.053 mmol) was dissolved in DCM (0.6 mL). *N*,*N*-Dimethyl-*p*-toluidine-*N*-oxide (0.012 g, 0.081 mmol) was added to the resulting solution, and the reaction mixture was stirred for 1 h. The solvent was removed under reduced pressure, and the crude product was purified by flash column chromatography (15% v/v EtOAc in hexanes) to afford compound **3** as a pale-yellow solid (0.010 g, 70%) with mp >400 °C. ^{1}H NMR (500 MHz, CD_3OD, δ): 6.18−6.19 (t, J = 2.15 Hz, 1H), 6.47 (s, 2H), 6.74−6.76 (d, J = 8.66 Hz, 1H), 6.82 (s, 1H), 6.82−6.85 (d, J = 14.57 Hz, 1H), 7.31−7.34 (d, J = 16.16 Hz, 1H), 7.58−7.59 (d, J = 8.64 Hz, 1H). ^{13}C NMR (125 MHz, CD_3OD, δ): 103.10, 105.96, 115.92, 117.03, 124.95, 127.75, 128.32, 129.78, 134.77, 140.91, 159.08, 159.77. HRMS−ESI (m/z): $[M - H]^-$ calcd for $C_{14}H_{11}ClO_3$, 261.0324; found, 261.0325.

*5-[(1E)-2-(2-Chloro-4-boronic acid)ethenyl]-1,3-benzenediol (**4**).* Compound **3c** (0.050 g, 0.134 mmol) was dissolved in 4:1 THF/H_2O (1.3 mL). $NaIO_4$ (0.143 g, 0.670 mmol) was added to the resulting solution, followed by 1.0 M HCl (33 μL, 0.033 mmol). The reaction mixture was then stirred overnight. The reaction mixture was diluted with H_2O (1.0 mL) and extracted with EtOAc (3 × 2 mL). The organic layers were combined and washed with brine (6 mL), dried with Na_2SO_4(s), and filtered. The solvent was removed under reduced pressure, and the crude mixture was purified by flash column chromatography (4% v/v CH_3OH in DCM) to afford compound **4** as a white crystalline solid (0.022 g, 88%) with mp 186.0 °C. ^{1}H NMR (500 MHz, CD_3OD, δ): 6.23 (s, 1H), 6.52 (s, 2H), 7.05−7.09 (d, J = 16.20 Hz, 1H), 7.41−7.45 (d, J = 16.23 Hz, 1H), 7.54−7.56 (d, J = 7.85 Hz, 1H), 7.63 (s, 1H), 7.75−7.76 (d, J = 7.81 Hz, 1H). ^{13}C NMR (125 MHz, CD_3OD, δ): 103.77, 106.32, 124.88, 126.71, 133.26, 133.34, 133.90, 135.91, 137.59, 140.29, 159.89. HRMS−ESI (m/z): $[M - H]^-$ calcd for $C_{14}H_{12}BClO_4$, 288.0481; found, 288.0482.

*3-[(1E)-2-(4-Bromophenyl)ethenyl]benzoic Acid Methyl Ester (**5a**).* Ethyl 3-(bromomethyl)benzoate (2.0 g, 8.7 mmol) was dissolved in neat triethylphosphite (1.78 mL, 10.4 mmol) and heated to 150 °C for 4 h. The reaction mixture was cooled to 0 °C and diluted with DMF (87 mL). NaH (60% w/v in mineral oil, 0.69 g, 17.46 mmol) was added to the resulting solution, and the reaction mixture stirred at 0 °C for 20 min. A solution of 4-bromobenzaldehyde (1.62 g, 8.73 mmol) in DMF (87 mL) was then added dropwise. The reaction mixture was allowed to warm to room temperature and stirred overnight. The reaction mixture was then diluted with EtOAc (50 mL) and washed with 10% w/v citric acid (20 mL), followed by brine (20 mL). The organic layer was separated, dried with Na_2SO_4(s), and filtered. The solvent was removed under reduced pressure, and the crude product was purified by flash column chromatography (10% v/v EtOAc in hexanes) to afford the **5a** as a white solid (1.75 g, 63% over 2 steps). ^{1}H NMR (500 MHz, CD_3OD, δ): 3.84 (s, 3H), 6.94−6.96 (d, J = 8.70 Hz, 2H), 7.09−7.12 (d, J = 16.28, 1H), 7.20−7.25 (d, J = 16.41 Hz, 1H), 7.45−7.48 (t, J = 7.67, 1H), 7.53−7.55 (d, J = 8.62 Hz, 2H), 7.76−7.78 (d, J = 7.85 Hz, 1H), 7.88−7.90 (d, J = 7.72, 1H), 8.18 (s, 1H). ^{13}C NMR (125 MHz, CD_3OD, δ): 54.31, 113.73, 124.97, 126.93, 127.58, 127.80, 128.40, 129.13, 130.01, 138.21, 159.72, 168.62. HRMS−ESI (m/z): $M^{+\bullet}$ calcd for $C_{16}H_{13}BrO_2$, 316.0094; found, 316.0081.

*3-[(1E)-2-(4-Bromophenyl)ethenyl]benzoic Acid (**5b**).* Compound **5a** (1.5 g, 4.7 mmol) was dissolved in 3:1 THF/EtOH (47 mL). A solution of 2 M NaOH (4.7 mL, 9.4 mmol) was added to the resulting solution, and the reaction mixture was stirred overnight. The reaction mixture was then diluted with EtOAc (20 mL) and washed with 10% w/v citric acid (20 mL), followed by brine (20 mL). The organic layer was separated, dried with Na_2SO_4(s), and filtered. The solvent was removed under reduced pressure, and the crude product was purified by flash column chromatography (20% v/v EtOAc in hexanes) to afford compound **5b** as a white solid (1.36 g, 96%). ^{1}H NMR (500 MHz, DMSO, δ): 7.33−7.36 (d, J = 16.52 Hz, 1H), 7.40−7.43 (d, J = 16.44 Hz, 1H), 7.50−7.54 (t, J = 7.68 Hz, 1H), 7.58−7.60 (d, J = 8.64 Hz, 2H), 7.63−7.61 (d, J = 8.66 Hz, 2H), 7.84−7.88 (t, J = 8.63 Hz, 2H), 8.16 (s, 1H), 13.10 (s, 1H). ^{13}C NMR (125 MHz, DMSO, δ): 121.27, 127.81, 128.68, 128.92, 129.00, 129.10, 129.51, 131.04, 132.09, 136.61, 137.66, 167.69. HRMS−ESI (m/z): $M^{+\bullet}$ calcd for $C_{15}H_{11}BrO_2$, 301.9937; found, 301.9944.

*3-[(1E)-2-(4-Boronic acid pinacol ester)ethenyl]benzoic Acid (**5c**).* Compound **5b** (1.0 g, 3.3 mmol), KOAc (0.971 g, 9.9 mmol), bis(pinacolato)diboron (2.5 g, 9.9 mmol), and Pd(dppf)Cl_2 (0.24 g, 0.33 mmol) were added to a flame-dried Schlenk flask, which was then evacuated and backfilled with N_2(g). Dioxane (33 mL) was deoxygenated by sonication under high vacuum and backfilled with N_2(g). The deoxygenated dioxane was then added by cannula into the reaction flask, and the reaction mixture was stirred overnight at 80 °C. The reaction mixture was filtered, and the solvent was removed under reduced pressure. The crude product was purified by flash column chromatography (20% v/v EtOAc in hexanes) to afford compound **5c** as a white solid (0.850 g, 73%). ^{1}H NMR (500 MHz, $CDCl_3$, δ): 1.36, (s, 12H), 7.22 (s, 2H), 7.46−7.50 (t, J = 7.44 Hz, 1H), 7.54−7.55 (d, J = 7.72 Hz, 1H), 7.76−7.77 (d, J = 8.12 Hz, 2H), 7.81−7.83 (d, J = 8.10 Hz, 2H), 8.00−8.01 (d, J = 8.11 Hz, 1H), 8.27−8.28 (d, J = 7.72 Hz, 1H), 8.28 (s, 1H). ^{13}C NMR (125 MHz, $CDCl_3$, δ): 24.90, 83.87, 125.97, 128.19, 128.32, 128.94, 129.28, 129.70, 130.06, 131.67, 135.23, 137.70, 139.50. HRMS−ESI (m/z): $[M + NH_4]^+$ calcd for $C_{21}H_{23}BO_4$, 367.2064; found, 367.2062.

*3-[(1E)-2-(4-Hydroxyphenyl)ethenyl]benzoic Acid (**5**).* Compound **5c** (0.050 g, 0.142 mmol) was dissolved in DCM (1.4 mL). *N*,*N*-Dimethyl-*p*-toluidine-*N*-oxide (0.032 g, 0.213 mmol) was added to the resulting solution, and the reaction mixture was allowed to stir for 1 h.

DOI: 10.1021/acs.jmedchem.7b00952
J. Med. Chem. 2017, 60, 7820−7834

The reaction mixture was filtered, and the solvent was removed under reduced pressure. The crude product was purified by flash column chromatography (2% v/v MeOH in DCM) to afford compound **5** as a white solid (0.030 g, 88%) with mp >400 °C. ^{1}H NMR (500 MHz, CD_3OD, δ): 6.78−6.80 (d, J = 8.61 Hz, 2H), 7.02−7.05 (d, J = 16.32 Hz, 1H), 7.15−7.19 (d, J = 16.34 Hz, 1H), 7.42−7.44 (d, J = 8.26 Hz, 2H), 7.42−7.45 (t, J = 7.28 Hz, 1H), 7.73−7.75 (d, J = 7.82 Hz, 1H), 7.85−7.87 (d, J = 7.79 Hz, 1H), 8.15 (s, 1H). ^{13}C NMR (125 MHz, CD_3OD, δ): 116.52, 125.56, 128.25, 129.04, 129.10, 129.80, 130.04, 130.90, 131.42, 132.30, 139.80. HRMS−ESI (m/z): $[M - H]^-$ calcd for $C_{15}H_{12}O_3$, 239.0714; found, 239.0716.

*3-[(1E)-2-(4-Boronic acid)ethenyl]benzoic Acid (**6**).* Compound **5c** (0.5 g, 1.48 mmol) was dissolved in 4:1 THF/H_2O (15 mL). $NaIO_4$ (0.405 g, 1.89 mmol) was added to the resulting solution, followed by 1.0 M HCl (0.15 mL, 0.158 mmol). The reaction mixture was then stirred overnight. The reaction mixture was diluted with H_2O (10 mL) and extracted with EtOAc (3 × 15 mL). The organic layers were combined and washed with brine (20 mL), dried with Na_2SO_4(s), and filtered. The solvent was removed under reduced pressure, and the crude product was purified by flash column chromatography (10% v/v CH_3OH in DCM) to afford compound **6** as a white crystalline solid (0.345 g, 90%) with mp 174.2 °C. ^{1}H NMR (500 MHz, $CDCl_3$, δ): 7.24−7.27 (d, J = 16.43 Hz, 1H), 7.28−7.32 (d, J = 16.45 Hz, 1H), 7.49−7.76 (t, J = 7.70 Hz, 1H), 7.58−7.59 (d, J = 7.94 Hz, 2H), 7.62−7.64 (d, J = 7.92 Hz, 2H), 7.80−7.82 (d, J = 7.87 Hz, 1H), 7.90−7.92 (d, J = 7.81 Hz, 1H), 8.21 (s, 1H). ^{13}C NMR (125 MHz, $CDCl_3$, δ): 125.51, 127.32, 127.86, 128.37, 128.51, 129.41, 130.43, 131.07, 133.70, 137.77, 138.27, 168.32. HRMS−ESI (m/z): $[M - H]^-$ calcd for single methyl boronic acid $C_{16}H_{15}BO_4$, 280.1026; found, 280.1033.

*Methyl 4-Bromo-2-chlorobenzoate (**7a**).* 4-Bromo-2-chlorotoluene (1.0 g, 4.8 mmol) was dissolved in 1:1 water/*tert*-butanol (20 mL). $KMnO_4$ (1.53 g, 9.7 mmol) was added to the resulting solution, and the reaction mixture was heated to 70 °C with a reflux condenser for 2 h. The reaction mixture was then allowed to cool to room temperature, and more $KMnO_4$ (1.53 g, 9.7 mmol) was added. The reaction mixture was then reheated to 70 °C in a flask with a reflux condenser and stirred overnight at 70 °C. The warm reaction mixture was filtered, and the resulting $KMnO_4$ cake was rinsed with water (~10 mL). The filtrate was acidified to pH 3 with concentrated HCl and extracted with EtOAc (3 × 20 mL). The organic layers were combined, dried with $NaSO_4$(s), and filtered. The solvent was removed under reduced pressure to afford the carboxylic acid precursor as a white solid. This precursor was dissolved in 3 M HCl in MeOH (15 mL) and heated to reflux for 12 h. The reaction mixture was allowed to cool to room temperature, and N_2(g) was bubbled through the solution for 20 min to remove excess HCl(g). The solvent was removed under reduced pressure, and the crude product was purified by flash column chromatography (20% v/v EtOAc in hexanes) to afford compound **7a** as a colorless oil (1.15 g, 96% yield over 2 steps). ^{1}H NMR (500 MHz, CD_3OD, δ): 3.93 (s, 3H), 7.59−7.61 (d, J = 8.47 Hz, 1H), 7.76−7.77 (m, 2H). ^{13}C NMR (125 MHz, CD_3OD, δ): 53.07, 127.34, 130.51, 131.41, 133.71, 134.63, 135.53, 166.72. HRMS−ESI (m/z): $M^{+\bullet}$ calcd for $C_8H_6BrClO_2$, 247.9235; found, 247.9237.

*4-Bromo-2-chlorobenzyl Alcohol (**7b**).* Compound **7a** (1.00 g, 4.01 mmol) was dissolved in THF (47 mL), and the resulting solution was cooled to 0 °C. Then 2 M $LiBH_4$ in THF (12 mL, 23.5 mmol) were added dropwise, followed by methanol (4 mL). The reaction mixture was allowed to warm to room temperature and stirred overnight. The reaction mixture was quenched by adding EtOAc (20 mL) dropwise, followed by water (15 mL) and then acidification to pH 5 with 1.0 M HCl. The resulting lithium salts were removed by filtration, and the filtrate was extracted with EtOAc (3 × 15 mL). The organic layers were combined, dried with $NaSO_4$(s), and filtered. The solvent was removed under reduced pressure, and the crude product was purified by flash column chromatography (20% v/v EtOAc in hexanes) to afford compound **7b** as a white solid (0.843 g, 95%). ^{1}H NMR (500 MHz, $CDCl_3$, δ): 1.91 (bs, 1H), 4.74 (s, 2H), 7.38−7.39 (d, J = 8.22 Hz, 1H), 7.42−7.44 (d, J = 8.23, 1H) 7.53 (s, 1H). ^{13}C NMR (500 MHz, $CDCl_3$, δ): 62.48, 121.68, 129.93, 130.42, 132.05, 133.54, 137.43. HRMS−ESI (m/z): $M^{+\bullet}$ calcd for C_7H_6OBrCl, 219.9286; found, 219.9282.

*4-Bromo-2-chlorobenzaldehyde (**7c**).* Compound **7b** (0.5 g, 2.28 mmol) was dissolved in DCM (22 mL). Pyridinium dichromate (PDC, 2.57 g, 6.84 mmol) was added to the resulting solution, and the reaction mixture was allowed to stir overnight. The reaction mixture was then filtered through a pad of Celite, and the solvent was removed under reduced pressure. The crude product was purified by flash column chromatography (10% v/v EtOAc in hexanes) to afford compound **7c** as a white solid (0.440 g, 88%). ^{1}H NMR (500 MHz, $CDCl_3$, δ): 7.54−7.55 (d, J = 8.25 Hz, 1H), 7.66 (s, 1H), 7.78−7.80 (d, J = 8.32 Hz, 1H), 10.42 (s, 1H). ^{13}C NMR (125 MHz, $CDCl_3$, δ) 129.78, 130.55, 131.09, 131.45, 133.49, 138.71, 188.95. ASAP−MS (m/z): $[M + H]^+$ calcd for C_7H_4BrClO, 218.9207; found, 218.9216.

*3-[(1E)-2-(2-Chloro-4-bromophenyl)ethenyl]benzoic Acid Methyl Ester (**7d**).* Ethyl 3-(bromomethyl)benzoate (1.04 g, 4.55 mmol) was dissolved in neat triethylphosphite (0.9 mL, 5.46 mmol), and the resulting solution was heated to 150 °C for 4 h. The reaction mixture was cooled to 0 °C and diluted with DMF (40 mL). NaH (60% w/v in mineral oil, 0.23 g, 5.91 mmol) was added to the resulting solution, and the reaction mixture was stirred at 0 °C for 20 min. A solution of 4-bromo-2-chlorobenzaldehyde (**7c**; 1.0 g, 4.6 mmol) in DMF (5 mL) was added dropwise. The reaction mixture was then allowed to warm to room temperature and stirred overnight. The reaction mixture was diluted with EtOAc (5 mL), and washed with 10% w/v citric acid (5 mL), followed by brine (5 mL). The organic layer was separated, dried with Na_2SO_4(s), and filtered. The solvent was removed under reduced pressure, and the crude product was purified by flash column chromatography (10% v/v EtOAc in hexanes) to afford compound **7d** as a white solid (1.3 g, 83% over 2 steps). ^{1}H NMR (500 MHz, $CDCl_3$, δ): 3.95 (s, 3H), 7.08−7.11 (d, J = 16.31 Hz, 1H), 7.39−7.41 (d, J = 8.53 Hz, 1H), 7.44−7.47 (t, J = 8.02 Hz, 1H), 7.45−7.49 (d, J = 16.56 Hz, 1H), 7.53−7.55 (d, J = 8.45 Hz, 1H), 7.56 (s, 1H), 7.71−7.73 (d, J = 7.73 Hz, 1H), 7.96−7.97 (d, J = 7.70 Hz, 1H), 8.19 (s, 1H). ^{13}C NMR (125 MHz, $CDCl_3$, δ): 52.43, 121.70, 125.02, 127.66, 128.15, 129.02, 129.35, 130.39, 130.88, 131.12, 132.55, 134.26, 134.35, 137.19, 167.02. HRMS−ESI (m/z): $[M + NH_4]^+$ calcd for $C_{16}H_{12}BrClO_2$, 368.0048; found, 368.0053.

*3-[(1E)-2-(2-Chloro-4-bromophenyl)ethenyl]benzoic Acid (**7e**).* Compound **7d** (1.34 g, 3.83 mmol) was dissolved in 3:1 THF/EtOH (40 mL). Then 2.0 M NaOH (3.3 mL, 7.7 mmol) was added to the resulting solution, and the reaction mixture was stirred overnight. The reaction mixture was diluted with EtOAc (20 mL) and washed with 10% w/v citric acid (30 mL), followed by brine (30 mL). The organic layer was separated, dried with Na_2SO_4(s), and filtered. The solvent was removed under reduced pressure, and the crude product was purified by flash column chromatography (20% v/v EtOAc in hexanes) to afford compound **7e** as a white solid (1.22 g, 95%). ^{1}H NMR (500 MHz, DMSO, δ): 7.42−7.45 (d, J = 16.39 Hz, 1H), 7.47−7.50 (d, J = 16.41 Hz, 1H), 7.53−7.56 (t, J = 7.71 Hz, 1H), 7.60−7.62 (d, J = 8.54, 1H), 7.79 (s, 1H), 7.86−7.88 (d, J = 8.63 Hz, 1H), 7.88−7.92 (t, J = 7.86, 2H), 8.15 (s, 1H), 13.01 (bs, 1H). ^{13}C NMR (125 MHz, DMSO, δ): 121.99, 124.85, 128.89, 129.10, 129.94, 130.17, 131.41, 131.73, 132.08, 132.38, 132.87, 134.61, 135.22, 138.07, 167.31. HRMS−ESI (m/z): $[M - H]^-$ calcd for $C_{15}H_{10}BrClO_2$, 334.9479; found, 334.9476.

*3-[(1E)-2-(2-Chloro-4-boronic acid pinacol ester)ethenyl]benzoic Acid (**7f**).* Compound **7e** (0.200 g, 0.580 mmol), KOAc (0.171 g, 1.791 mmol), bis(pinacolato)diboron (0.45 g, 1.79 mmol), and $Pd(dppf)Cl_2$ (0.043 g, 0.059 mmol) were added to a flame-dried Schlenk flask, which was then evacuated and backfilled with N_2(g). Dioxane (6 mL) was deoxygenated by sonication under high vacuum and backfilled with N_2(g). The deoxygenated dioxane was then added by cannula into the reaction flask, and the reaction mixture was stirred overnight at 80 °C. The reaction mixture was filtered, and the solvent was removed under reduced pressure. The crude product was purified by flash column chromatography (1% v/v CH_3OH in DCM) to afford compound **7f** as a white solid (0.183 g, 82%). ^{1}H NMR (500 MHz, CD_3OD, δ): 1.36 (s, 12H), 7.33−7.36 (d, J = 16.30 Hz, 1H), 7.49−7.52 (t, J = 8.41 Hz, 1H), 7.61−7.64 (d, J = 16.47 Hz, 1H), 7.66−7.67

DOI: 10.1021/acs.jmedchem.7b00952
J. Med. Chem. 2017, 60, 7820−7834

(d, J = 7.46, 1H), 7.73 (s, 1H), 7.83−7.85 (d, J = 7.75 Hz, 2H), 7.95−7.97 (d, J = 7.73, 1H), 8.24 (s, 1H). ^{13}C NMR (125 MHz, CD_3OD, δ): 25.19, 85.51, 126.33, 127.18, 129.00, 130.07, 130.41, 132.16, 132.61, 134.18, 136.79, 138.74, 138.86, 169.56. HRMS−ESI (m/z): $[M + NH_4]^+$ calcd for $C_{21}H_{22}BClO_4$, 401.1675; found, 401.1666.

*3-[(1E)-2-(2-Chloro-4-hydroxyphenyl)ethenyl]benzoic Acid (**7**).* Compound **7f** (0.100 g, 0.259 mmol) was dissolved in DCM (2.6 mL). *N*,*N*-Dimethyl-*p*-toluidine-*N*-oxide (0.060 g, 0.389 mmol) was added to the resulting solution, and the reaction mixture was then stirred overnight. The solvent was removed under reduced pressure, and the crude product was purified by flash column chromatography (2% v/v MeOH in DCM) to afford compound **7** as a white solid (0.051 g, 72%) with mp 213.6 °C. ^{1}H NMR (500 MHz, CD_3OD, δ): 6.77−6.68 (d, J = 8.63 Hz, 1H), 6.84 (s, 1H), 7.06−7.10 (d, J = 16.34 Hz, 1H), 7.45−7.48 (t, J = 7.72 Hz, 1H), 7.49−7.52 (d, J = 16.31 Hz, 1H), 7.65−7.67 (d, J = 8.63 Hz, 1H), 7.75−7.77 (d, J = 7.91 Hz, 1H), 7.89−7.91 (d, J = 7.78 Hz, 1H), 8.17 (s, 1H). ^{13}C NMR (125 MHz, CD_3OD, δ): 115.98, 117.09, 126.42, 127.43, 128.47, 128.48, 128.58, 129.60, 129.92, 131.70, 132.43, 135.06, 139.41, 159.45, 169.74. HRMS−ESI (m/z): $[M - H]^-$ calcd for $C_{15}H_{11}ClO_3$, 273.0324; found, 273.0327.

*3-[(1E)-2-(2-Chloro-4-boronic acid)ethenyl]benzoic Acid (**8**).* Compound **7f** (0.100 g, 0.260 mmol) was dissolved in 4:1 THF/H_2O (2.6 mL). $NaIO_4$ (0.28 g, 1.30 mmol) was added to the resulting solution, followed by 0.02 mL of 1.0 M HCl (0.02 mmol). The reaction mixture was then stirred overnight. The reaction mixture was diluted with H_2O (2 mL) and extracted with EtOAc (3 × 3 mL). The organic layers were combined and washed with brine (5 mL), dried with Na_2SO_4(s), and filtered. The solvent was removed under reduced pressure, and the crude product was purified by flash column chromatography (1−3% v/v CH_3OH in DCM) to afford compound **8** as a white crystalline solid (0.058 g, 75%) with mp 161.0 °C. ^{1}H NMR (500 MHz, CD_3OD, δ): 7.32−7.35 (d, J = 16.37 Hz, 1H), 7.51−7.54 (t, J = 7.73 Hz, 1H), 7.51−7.67 (m, 3H), 7.84−7.85 (d, J = 7.29 Hz, 2H), 7.97−7.98 (d, J = 7.76 Hz, 1H), 8.25 (s, 1H). ^{13}C NMR (125 MHz, CD_3OD, δ): 126.41, 126.94, 128.93, 130.04, 130.29, 132.07, 132.63, 133.31, 134.12, 135.95, 137.29, 138.82, 169.61. HRMS−ESI (m/z): $[M - H]^-$ calcd for the single methyl boronic ester $C_{16}H_{14}BClO_4$, 314.0637; found, 314.0635.

*1,1′-(1E)-(1,2-Ethenediyl)bis[2-chloro-4-bromo]benzene (**9a**).* 4-Bromo-1-(bromomethyl)-2-chlorobenzene (0.300 g, 1.05 mmol) was dissolved in neat triethylphosphite (0.217 mL, 1.26 mmol) and heated to 150 °C for 4 h. The reaction mixture was then cooled to 0 °C and diluted with DMF (8 mL). NaH (60% w/v in mineral oil, 0.054 g, 1.36 mmol) was added to the resulting solution, and the reaction mixture was stirred at 0 °C for 20 min. A solution of 4-bromo-2-chlorobenzaldehyde (**7c**; 0.230 g, 1.05 mmol) in DMF (2.5 mL) was then added dropwise. The reaction mixture was allowed to warm to room temperature and stirred overnight. The reaction mixture was diluted with EtOAc (8 mL) and washed with 10% w/v citric acid (10 mL), followed by brine (10 mL). The organic layer was then separated, dried with Na_2SO_4(s), and filtered. The solvent was removed under reduced pressure, and the crude product was suspended in cold DCM (10 mL). The resulting precipitate was collected by filtration to afford compound **9a** as a white solid (0.306 g, 72% yield over 2 steps). ^{1}H NMR (500 MHz, $CDCl_3$, δ): 7.39 (s, 2H), 7.41−7.43 (d, J = 8.42 Hz, 2H), 7.58 (s, 2H), 7.58−7.59 (d, J = 7.12 Hz, 2H). ^{13}C NMR (125 MHz, $CDCl_3$, δ): 121.99, 126.70, 127.83, 130.35, 132.45, 133.89, 134.30. ASAP−MS (m/z): $M^{+\bullet}$ calcd for $C_{14}H_8Br_2Cl_2$, 403.8365; found, 403.8367.

*1,1′-(1E)-(1,2-Ethenediyl)bis[2-chloro-4-boronic acid pinacol ester]benzene (**9b**).* Compound **9a** (0.050 g, 0.123 mmol), KOAc (0.071 g, 0.742 mmol), bis(pinacolato)diboron (0.187 g, 0.742 mmol), and Pd(dppf)Cl_2 (9 mg, 0.012 mmol) were added to a flame-dried Schlenk flask, which was then evacuated and backfilled with N_2(g). Dioxane (2 mL) was deoxygenated by sonication under high vacuum and backfilled with N_2(g). The deoxygenated dioxane was then added by cannula into the reaction flask, and the reaction mixture was heated to 80 °C and stirred overnight (Note: higher yields of the diboronated product were found at more dilute reaction concentrations). The reaction mixture was filtered, and the solvent was removed under reduced pressure. The crude product was purified by flash column chromatography (50% v/v DCM in hexanes) to afford **9b** as a white solid (0.056 g, 92%). ^{1}H NMR (500 MHz, $CDCl_3$, δ): 1.35 (s, 24H), 7.56 (s, 2H), 7.67−7.69 (d, J = 7.76 Hz, 2H), 7.73−7.75 (d, J = 7.85 Hz, 2H), 7.83 (s, 2H). ^{13}C NMR (125 MHz, $CDCl_3$, δ): 24.88, 84.18, 126.17, 127.94, 133.02, 133.45, 136.06, 137.45. ASAP−MS (m/z): $[M + H]^+$ calcd for $C_{26}H_{32}B_2Cl_2O_4$, 499.2009; found, 499.2001.

*1,1′-(1E)-(1,2-Ethenediyl)bis[2-chloro-4-hydroxy]benzene (**9**).* Compound **9b** (0.020 g, 0.040 mmol) was dissolved in DCM (0.5 mL). *N*,*N*-Dimethyl-*p*-toluidine-*N*-oxide (0.018 g, 0.120 mmol) was added to the resulting solution, and the reaction mixture was stirred for 1 h. The solvent was removed under reduced pressure, and the crude product was purified by flash column chromatography (2% v/v MeOH in DCM) to afford compound **9** as a white solid (9 mg, 80%) with mp 203.9 °C. ^{1}H NMR (500 MHz, CD_3OD, δ): 6.75−6.77 (d, J = 8.61 Hz, 2H), 6.83 (s, 2H), 7.24 (s, 2H), 7.55−7.57 (d, J = 8.59 Hz, 2H). ^{13}C NMR (125 MHz, CD_3OD, δ): 115.93, 117.07, 125.22, 128.00, 128.36, 134.73, 159.09. HRMS−ESI (m/z): $[M - H]^-$ calcd for $C_{14}H_{10}Cl_2O_2$, 278.9985; found, 278.9985.

*1,1′-(1E)-(1,2-Ethenediyl)bis[2-chloro-4-boronic acid]benzene (**10**).* Compound **9b** (0.020 g, 0.040 mmol) was dissolved in 4:1 THF/H_2O (0.6 mL). $NaIO_4$ (0.042 g, 0.200 mmol) was added to the resulting solution, followed by a few drops of 1.0 M HCl. The reaction mixture was then stirred overnight. The reaction mixture was then diluted with H_2O (1 mL) and extracted with EtOAc (3 × 2 mL). The organic layers were combined and washed with saturated brine (3 mL), dried with Na_2SO_4(s), and filtered. The solvent was removed under reduced pressure, and the crude product was purified by flash column chromatography (3% v/v CH_3OH in DCM) to afford compound **10** as a white crystalline solid (0.010 g, 74%) with mp 234.2 °C. ^{1}H NMR (500 MHz, CD_3OD, δ): 7.59 (s, 1H), 7.59−7.60 (d, J = 8.42 Hz, 2H), 7.66 (s, 1H), 7.78−7.80 (d, J = 7.78 Hz, 2H). ^{13}C NMR (125 MHz, CD_3OD, δ): 127.14, 128.69, 133.38, 134.25, 135.98. MALDI−MS (m/z): $M^{+\bullet}$ calcd for $C_{14}H_{12}B_2Cl_2O_4$, 336.03; found, 336.00.

*2-Bromo-1-[(1E)-2-(3-bromophenyl)ethenyl]-4-chlorobenzene (**11a**).* 3-Bromobenzyl bromide (0.500 g, 2.00 mmol) was dissolved in neat triethylphosphite (0.411 mL, 2.4 mmol), and the resulting solution was heated to 150 °C for 4 h. The reaction mixture was cooled to 0 °C and then diluted with DMF (10 mL). NaH (60% w/v in mineral oil, 0.096 g, 2.4 mmol) was added to the resulting solution, and the reaction mixture stirred at 0 °C for 20 min. A solution of 4-bromo-2-chlorobenzaldehyde (**7c**; 0.447 g, 2.04 mmol) in DMF (10 mL) was then added dropwise. The reaction mixture was allowed to warm to room temperature and stirred overnight. The reaction mixture was diluted with EtOAc (20 mL) and washed with 10% w/v citric acid (30 mL) followed by brine (30 mL). The organic layer was separated, dried with Na_2SO_4(s), and filtered. The solvent was removed under reduced pressure, and the crude product was suspended in ice-cold DCM (5 mL). The resulting precipitate was collected by filtration to afford compound **11a** as a white solid (0.514 g, 69% over 2 steps). ^{1}H NMR (500 MHz, CD_3OD, δ): 7.09−7.13 (d, J = 16.3 Hz, 1H), 7.26−7.29 (d, J = 12.53 Hz, 2H), 7.35−7.39 (t, J = 7.61 Hz, 1H), 7.53 (s, 3H), 7.61−7.63 (d, J = 7.74 Hz, 1H), 7.79 (s, 1H). ^{13}C NMR (125 MHz, CD_3OD, δ): 124.42, 125.32, 126.40, 127.54, 127.67, 131.61, 131.80, 131.80, 132.97, 134.94, 135.71, 141.09. ASAP−MS (m/z): $M^{+\bullet}$ calcd for $C_{14}H_9Br_2Cl$, 369.8754; found, 369.8740.

*2-Boronic Acid Pinacol Ester-1-[(1E)-2-(3-boronic acid pinacol ester)ethenyl]-4-chlorobenzene (**11b**).* Compound **11a** (0.100 g, 0.270 mmol), KOAc (0.152 g, 1.62 mmol), bis(pinacolato)diboron (0.410 g, 1.62 mmol), and Pd(dppf)Cl_2 (0.0270 g, 0.020 mmol) were added to a flame-dried Schlenk flask, which was then evacuated and backfilled with N_2(g). Dioxane (3.6 mL) was deoxygenated by sonication under high vacuum and backfilled with N_2(g). The deoxygenated dioxane was then added by cannula into the reaction flask, and the reaction mixture was heated to 80 °C and stirred overnight. The reaction mixture was filtered, and the solvent was removed under reduced pressure. The crude product was purified by

DOI: 10.1021/acs.jmedchem.7b00952
J. Med. Chem. 2017, 60, 7820−7834

flash column chromatography (2% v/v DCM in hexanes) to afford **11b** as a white solid (0.111 g, 87%). ^{1}H NMR (500 MHz, CD_3OD, δ): 1.36 (s, 12H), 1.38 (s, 12H), 7.27−7.30 (d, J = 16.29 Hz, 1H), 7.38−7.41 (t, J = 7.47 Hz, 1H), 7.55−7.58 (d, J = 16.30 Hz, 1H), 7.64−7.66 (d, J = 7.73 Hz, 1H), 7.67−7.70 (t, J = 7.88 Hz, 2H), 7.72 (s, 1H), 7.81−7.82 (d, J = 7.75 Hz, 1H), 7.96 (s, 1H). ^{13}C NMR (125 MHz, CD_3OD, δ): 26.45, 26.48, 50.43, 50.60, 86.55, 86.74, 126.43, 128.29, 130.59, 132.18, 134.79, 135.29, 135.31, 135.40, 136.90, 138.03, 138.91, 140.44. HRMS−ESI (m/z): $[M + NH_4]^+$ calcd for $C_{26}H_{33}B_2ClO_4$, 484.2607; found, 484.2600.

2-Boronic Acid-1-[(1E)-2-(3-boronic acid)ethenyl]-4-chlorobenzene (11). Compound **11b** (0.100 g, 0.214 mmol) was dissolved in 4:1 THF/H_2O (2.1 mL). $NaIO_4$ (0.227 g, 1.07 mmol) was added to the resulting solution, followed by a few drops of 1.0 M HCl. The reaction mixture was then stirred overnight. The reaction mixture was diluted with H_2O (2 mL) and extracted with EtOAc (3 × 2 mL). The organic layers were combined and washed with brine (4 mL), dried with Na_2SO_4(s), and filtered. The solvent was removed under reduced pressure, and the crude product was purified by flash column chromatography (2% v/v CH_3OH in DCM) to afford compound 11 as a white crystalline solid (0.040 g, 63%) with mp 146.3 °C. ^{1}H NMR (500 MHz, CD_3OD, δ): 7.24−7.27 (d, J = 16.3 Hz, 1H), 7.37−7.40 (t, J = 7.57 Hz, 1H), 7.52−7.57 (m, 3H), 7.63−7.64 (d, J = 4.84 Hz, 2H), 7.79 (s, 2H). ^{13}C NMR (125 MHz, CD_3OD, δ): 125.12, 126.78, 128.85, 129.02, 129.16, 129.80, 133.24, 133.95, 134.31, 135.93, 137.64. HRMS−ESI (m/z): $[M - H]^-$ calcd for the single methyl boronate ester $C_{15}H_{14}B_2ClO_4$, 315.0772; found, 315.0772.

Protein Expression and Purification. Plasmids that direct the expression of wild-type TTR and its V30M variant were prepared in the pET32b vector from Merck KGaA (Darmstadt, Germany) by standard methods.[76] To create the plasmid encoding V30M TTR, two double-stranded DNA fragments were prepared by PCR using complementary primers containing V30M-generating substitutions and gene-specific primers targeting opposite termini for assembly with the plasmid fragment. Wild-type TTR and its V30M variant were produced in *Escherichia coli* strain BL-21 from Merck KGaA cultured in Luria−Bertani medium containing ampicillin (200 μM) at 37 °C. Gene expression was induced when $OD_{600\ nm}$ reached ∼2.0, and cells were then grown for an additional 4 h at 37 °C. Cell pellets were resuspended in 20 mM Tris−HCl buffer, pH 7.4, containing EDTA (1.0 mM) and lysed with a high-pressure cell disruptor from Constant Systems (Kennesaw, GA). The soluble fraction was isolated by centrifugation for 10 min at 10500g and for 1 h at 30000g.

Wild-type TTR and its V30M variant were purified as described previously,[77] with minor modifications. The lysate was fractionated with aqueous ammonium sulfate at 60−85% saturation. The precipitate was dissolved in 20 mM Tris−HCl buffer, pH 7.8, containing EDTA (1.0 mM) and dialyzed overnight against this same buffer. The isolate was clarified at 30000g for 30 min, filtered, and applied to a Hitrap Q HP column from GE Healthcare Life Sciences (Pittsburgh, PA) that had been equilibrated with the dialysis buffer. TTR was eluted with the same buffer containing NaCl (1.0 M) and was subjected to gel-filtration chromatography on a Superdex 75 column from GE Healthcare Life Sciences (Pittsburgh, PA) that had been pre-equilibrated with 10 mM sodium phosphate buffer, pH 7.6, containing KCl (100 mM). Pure tetrameric TTR eluted at ∼0.6 column volumes as monitored by SDS−PAGE. The concentration of wild-type TTR and its V30M variant was determined from the $A_{280\ nm}$ by using $\varepsilon = 18.5 \times 10^3\ M^{-1}\ cm^{-1}$ and confirmed with a bicinchoninic acid (BCA) assay using a kit from Pierce Biotechnology (Rockford, IL).

Competitive Fluorescence Assay. Fluorescence measurements were performed with a Photon Technology International Quantamaster spectrofluorometer (Edison, NJ). Wild-type TTR was found to form a complex with ANS that has a K_d value of 3.2 μM (data not shown).[78] To determine the affinity for ligands, wild-type TTR tetramers (500 nM) were incubated in 2.00 mL of 10 mM sodium phosphate buffer, pH 7.6, containing KCl (100 mM) and ANS (5.0 μM) until the fluorescence signal (excitation, 410 nm; emission, 460 nm) was stable (∼30 min). A ligand (1 nM−10 μM) was then added in aliquots (5 μL) from a stock solution in dimethylformamide (DMF). The fluorescence intensity at each ligand concentration was recorded before adding the next dose. Control experiments with only the solvent (DMF) revealed that the fluorescence intensity dropped proportionally with the dilution factor. Accordingly, average intensities were adjusted for the dilution incurred upon adding ligand and were expressed as a percent change from the initial measurement. The final DMF concentration was 6.3% by volume after 27 additions of ligand.

The data did not fit well to the one- or two-site competitive binding models used previously to describe other systems.[78] The asymmetric behavior is likely a consequence of two distinct binding events and a modest decrease in fluorescence intensity resulting from the first ANS dissociation event. The steepest inflection point at higher ligand concentrations can be attributed to the half-maximal concentration required to compete ANS from the second binding site. The Prusoff−Cheng relation was used to account for this competition, resulting in a logistic equation:[79]

$$\%\Delta I = \%I_o + \frac{\%I_f - \%I_o}{\left(1 + 10^{n\left(\log\left(K_{d,2}\left(1+\frac{[ANS]}{K_{d,ANS}}\right)\right)-[ligand]\right)}\right)^S} \quad (1)$$

where $K_{d,2}$ is the equilibrium dissociation constant of the second site, n is the Hill coefficient, and S is the symmetry parameter. Values of $K_{d,2}$ were determined with Prism 6 software from Graphpad (La Jolla, CA) by holding constant the ligand concentration, ANS concentration, and $K_{d,ANS}$ = 3.2 μM and varying other parameters to maximize the value of R^2, which was >0.99 for all data sets. The value of $K_{d,2}$ = (373 ± 10) nM for the TTR·tafamidis complex determined with this method is similar to the value of $K_{d,2}$ = 278 nM determined with isothermal titration calorimetry.[21] Values of $K_{d,1}$ were not obtainable by this method, although modest inflection points were observed in the low nanomolar range (Supporting Information, Figure S1). Reported values of $K_{d,1}$ for other ligands fall within this range, however, our efforts to improve kinetic stabilization properties focus on reducing the $K_{d,2}$ value.

Fibril-Formation Assay. Light-scattering at 400 nm was used to assess the formation of fibrils under acidic conditions, as described previously.[80] In this assay, turbidity is assumed to be proportional to the mass of the protein converted to fibrils. Ligands (7.2 or 14.4 μM) were incubated with TTR tetramers (7.2 μM) for 30 min prior to 2-fold dilution with 50 mM sodium acetate buffer, pH 4.4, containing KCl (100 mM). Absorbance at 400 nm was measured 10 times with four replicates in clear, flat-bottomed, 96-well plates at 0 and 96 h using an M1000 plate reader from Tecan (Maennedorf, Switzerland). Percent fibril formation was calculated from the difference in the light scattering that accumulated after 96 h in ligand-containing wells versus wells containing only vehicle (DMF), using the equation

$$\%\text{fibril formation} = \frac{A_{400nm,ligand,96h} - A_{400nm,ligand,0h}}{A_{400nm,DMF,96h} - A_{400nm,DMF,0h}} \times 100\% \quad (2)$$

Standard deviations from the four replicates were propagated through this calculation.

Protein Crystallization and X-ray Structure Determination. Crystals were grown by vapor diffusion using a solution of wild-type TTR (∼6.0 mg/mL in 10 mM sodium phosphate buffer, pH 7.6, containing 100 mM KCl) and stilbenes **2**−**8**, **10**, or **11** (7.2 mM, added from a stock solution in DMF). Hanging drops (2 μL of solution containing protein and ligand plus 2 μL of mother liquor) were equilibrated with a reservoir of 1.0−1.3 M sodium citrate buffer, pH 5.5, containing glycerol (1−3% v/v).[5] Crystals appeared after 1−3 days. TTR precipitated in the presence of stilbene **9** (7.2 mM). Crystals were cryoprotected by brief transfer into a solution of 1.5 M sodium citrate buffer, pH 5.5, containing glycerol (10% v/v). Diffraction data were collected at Sector 21 of the Life Sciences Collaborative Access Team (LS-CAT) at the Advanced Photon Source of Argonne National Laboratory (Argonne, IL). Data were reduced

DOI: 10.1021/acs.jmedchem.7b00952
J. Med. Chem. 2017, 60, 7820−7834

using HKL2000 (Supporting Information, Tables S2–S10).[81] Boronate ester restraints were obtained by measuring the bond lengths and angles from 10 CSD small-molecule structures (Supporting Information, Table S1). Initial phases were obtained by molecular replacement using the protein atoms of Protein Data Bank (PDB) entry 2qgb as a model.[64] Refinement and model building were conducted with the programs Phenix and Coot (Supporting Information, Tables S2–S10 and Figures S4–S12).[82,83] Ligand models in idealized geometries were prepared with the program WebMO, and restraints were prepared in Phenix with the program eLBOW. Restraints generated by eLBOW were modified to impose planarity on the four carbon atoms in the olefin of the stilbene and on the carbon, boron, and two oxygen atoms in a boronic acid group. Short interatomic distances in TTR·ligand complexes are listed in Supporting Information, Table S11. Atomic coordinates and structure factors for all nine TTR·ligand complexes have been deposited in the PDB.

■ ASSOCIATED CONTENT

Supporting Information

The Supporting Information is available free of charge on the ACS Publications website at DOI: 10.1021/acs.jmedchem.7b00952.

Assay data, crystallographic data, HPLC traces for compounds **2**, **3**, and **5**, ^{1}H and ^{13}C NMR spectra of all synthetic compounds (PDF)

Molecular formula strings (CSV)

Accession Codes

TTR·**2** complex, 5u48; TTR·**3** complex, 5u49; TTR·**4** complex, 5u4a; TTR·**5** complex, 5u4b; TTR·**6** complex, 5u4c; TTR·**7** complex, 5u4d; TTR·**8** complex, 5u4e; TTR·**10** complex, 5u4f; TTR·**11** complex, 5u4g.

■ AUTHOR INFORMATION

Corresponding Authors

*For R.T.R.: phone, 617-258-6006; E-mail, rtraines@mit.edu.
*For K.T.F.: E-mail, forest@bact.wisc.edu.

ORCID

Ronald T. Raines: 0000-0001-7164-1719

Present Addresses

#For T.P.S.: Promega Biosciences, LLC, 277 Granada Drive, San Luis Obispo, California 93401, United States.
⊥For I.W.W. and R.T.R.: Department of Chemistry, Massachusetts Institute of Technology, 77 Massachusetts Avenue, Cambridge, Massachusetts 02139, United States.

Author Contributions

‖T.P.S. and I.W.W. contributed equally and are listed alphabetically.

Notes

The authors declare no competing financial interest.

■ ACKNOWLEDGMENTS

We are grateful to Drs. R. M. Murphy and C. L. Jenkins for contributive discussions. I.W.W. was supported by a Biotechnology Training Grant T32 GM008349 (NIH) and a Genentech Predoctoral Fellowship. This work was supported by grants R01 GM044783 (NIH) and MCB 1518160 (NSF), and made use of NMRFAM (University of Wisconsin–Madison), which is supported by grant P41 GM103399 (NIH).

■ ABBREVIATIONS USED

EDTA, ethylenediaminetetraacetic acid; FDA, Food and Drug Administration USA; PDB, Protein Data Bank; TTR, transthyretin; T4, thyroxin

■ REFERENCES

(1) Dobson, C. M. Protein folding and misfolding. *Nature* **2003**, *426*, 884–890.
(2) Chiti, F.; Dobson, C. M. Protein misfolding, functional amyloid, and human disease. *Annu. Rev. Biochem.* **2006**, *75*, 333–366.
(3) Knowles, T. P.; Vendruscolo, M.; Dobson, C. M. The amyloid state and its association with protein misfolding diseases. *Nat. Rev. Mol. Cell Biol.* **2014**, *15*, 384–396.
(4) Richardson, S. J. Cell and molecular biology of transthyretin and thyroid hormones. *Int. Rev. Cytol.* **2007**, *258*, 137–193.
(5) Klabunde, T.; Petrassi, H. M.; Oza, V. B.; Raman, P.; Kelly, J. W.; Sacchettini, J. C. Rational design of potent human transthyretin amyloid disease inhibitors. *Nat. Struct. Biol.* **2000**, *7*, 312–321.
(6) Hamilton, J. A.; Benson, M. D. Transthyretin: A review from a structural perspective. *Cell. Mol. Life Sci.* **2001**, *58*, 1491–1521.
(7) Hund, E. Familial amyloidotic polyneuropathy: Current and emerging treatment options for transthyretin-mediated amyloidosis. *Appl. Clin. Genet.* **2012**, *5*, 37–41.
(8) Yang, D. T.; Joshi, G.; Cho, P. Y.; Johnson, J. A.; Murphy, R. M. Transthyretin as both a sensor and a scavenger of β-amyloid oligomers. *Biochemistry* **2013**, *52*, 2849–2861.
(9) Stein, T. D.; Anders, N. J.; DeCarli, C.; Chan, S. L.; Mattson, M. P.; Johnson, J. A. Neutralization of transthyretin reverses the neuroprotective effects of secreted amyloid precursor protein (APP) in APPSW mice resulting in tau phosphorylation and loss of hippocampal neurons: Support for the amyloid hypothesis. *J. Neurosci.* **2004**, *24*, 7707–7717.
(10) Li, X.; Zhang, X.; Ladiwala, A. R. A.; Du, D.; Yadav, J. K.; Tessier, P. M.; Wright, P. E.; Kelly, J. W.; Buxbaum, J. N. Mechanisms of transthyretin inhibition of β-amyloid aggregation *in vitro*. *J. Neurosci.* **2013**, *33*, 19423–19433.
(11) Miller, D. W.; Dill, K. A. Ligand binding to proteins: The binding landscape model. *Protein Sci.* **1997**, *6*, 2166–2179.
(12) Celej, M. S. Protein stability induced by ligand binding correlates with changes in protein flexibility. *Protein Sci.* **2003**, *12*, 1496–1506.
(13) Martinez Molina, D.; Jafari, R.; Ignatushchenko, M.; Seki, T.; Larsson, E. A.; Dan, C.; Sreekumar, L.; Cao, Y.; Nordlund, P. Monitoring drug target engagement in cells and tissues using the cellular thermal shift assay. *Science* **2013**, *341*, 84–87.
(14) Hingorani, K. S.; Metcalf, M. C.; Deming, D. T.; Garman, S. C.; Powers, E. T.; Gierasch, L. M. Ligand-promoted protein folding by biased kinetic partitioning. *Nat. Chem. Biol.* **2017**, *13*, 369–371.
(15) O'Sullivan, C.; Tompson, F. W. LX.—Invertase: A contribution to the history of an enzyme or unorganised ferment. *J. Chem. Soc., Trans.* **1890**, *57*, 834–931.
(16) Nencetti, S.; Orlandini, E. TTR fibril formation inhibition: Is there a SAR? *Curr. Med. Chem.* **2012**, *19*, 2356–2379.
(17) Obici, L.; Merlini, G. An overview of drugs currently under investigation for the treatment of transthyretin-related hereditary amyloidosis. *Expert Opin. Invest. Drugs* **2014**, *23*, 1239–1251.
(18) Johnson, S. M.; Wiseman, R. L.; Sekijima, Y.; Green, N. S.; Adamski-Werner, S. L.; Kelly, J. W. Native state kinetic stabilization as a strategy to ameliorate protein misfolding diseases: A focus on the transthyretin amyloidoses. *Acc. Chem. Res.* **2005**, *38*, 911–921.
(19) Adamski-Werner, S. L.; Palaninathan, S. K.; Sacchettini, J. C.; Kelly, J. W. Diflunisal analogs stabilize the native state of transthyretin. Potent inhibition of amyloidogenesis. *J. Med. Chem.* **2004**, *47*, 355–374.
(20) Castano, A.; Helmke, S.; Alvarez, J.; Delisle, S.; Maurer, M. S. Diflunisal for ATTR cardiac amyloidosis. *Congestive Heart Failure* **2012**, *18*, 315–319.

DOI: 10.1021/acs.jmedchem.7b00952
J. Med. Chem. 2017, 60, 7820–7834

(21) Bulawa, C. E.; Connelly, S.; DeVit, M.; Wang, L.; Weigel, C.; Fleming, J. A.; Packman, J.; Powers, E. T.; Wiseman, R. L.; Foss, T. R.; Wilson, I. A.; Kelly, J. W.; Labaudinière, R. Tafamidis, a potent and selective transthyretin kinetic stabilizer that inhibits the amyloid cascade. *Proc. Natl. Acad. Sci. U. S. A.* **2012**, *109*, 9629−9634.
(22) Sekijima, Y. Recent progress in the understanding and treatment of transthyretin amyloidosis. *J. Clin. Pharm. Ther.* **2014**, *39*, 225−233.
(23) Scott, L. J. Tafamidis: A review of its use in familial amyloid polyneuropathy. *Drugs* **2014**, *74*, 1371−1378.
(24) Johnson, D. S.; Weerapana, E.; Cravatt, B. F. Strategies for discovering and derisking covalent, irreversible enzyme inhibitors. *Future Med. Chem.* **2010**, *2*, 949−964.
(25) Miller, R. M.; Taunton, J. Targeting protein kinases with selective and semipromiscuous covalent inhibitors. *Methods Enzymol.* **2014**, *548*, 93−116.
(26) Baillie, T. A. Targeted covalent inhibitors for drug design. *Angew. Chem., Int. Ed.* **2016**, *55*, 13408−13421.
(27) Johnson, S. M.; Connelly, S.; Fearns, C.; Powers, E. T.; Kelly, J. W. The transthyretin amyloidoses: From delineating the molecular mechanism of aggregation linked to pathology to a regulatory-agency−approved drug. *J. Mol. Biol.* **2012**, *421*, 185−203.
(28) Choi, S.; Connelly, S.; Reixach, N.; Wilson, I. A.; Kelly, J. W. Chemoselective small molecules that covalently modify one lysine in a non-enzyme protein in plasma. *Nat. Chem. Biol.* **2009**, *6*, 133−139.
(29) Choi, S.; Ong, D. S. T.; Kelly, J. W. A stilbene that binds selectively to transthyretin in cells and remains dark until it undergoes a chemoselective reaction to create a bright blue fluorescent conjugate. *J. Am. Chem. Soc.* **2010**, *132*, 16043−16051.
(30) Suh, E. H.; Liu, Y.; Connelly, S.; Genereux, J. C.; Wilson, I. A.; Kelly, J. W. Stilbene vinyl sulfonamides as fluorogenic sensors of and traceless covalent kinetic stabilizers of transthyretin that prevent amyloidogenesis. *J. Am. Chem. Soc.* **2013**, *135*, 17869−17880.
(31) Grimster, N. P.; Connelly, S.; Baranczak, A.; Dong, J.; Krasnova, L. B.; Sharpless, K. B.; Powers, E. T.; Wilson, I. A.; Kelly, J. W. Aromatic sulfonyl fluorides covalently kinetically stabilize transthyretin to prevent amyloidogenesis while affording a fluorescent conjugate. *J. Am. Chem. Soc.* **2013**, *135*, 5656−5668.
(32) Baranczak, A.; Liu, Y.; Connelly, S.; Du, W.-G. H.; Greiner, E. R.; Genereux, J. C.; Wiseman, R. L.; Eisele, Y. S.; Bradbury, N. C.; Dong, J.; Noodleman, L.; Sharpless, K. B.; Wilson, I. A.; Encalada, S. E.; Kelly, J. W. A fluorogenic aryl fluorosulfate for intraorganellar transthyretin imaging in living cells and in *Caenorhabditis elegans*. *J. Am. Chem. Soc.* **2015**, *137*, 7404−7414.
(33) Lorand, J. P.; Edwards, J. O. Polyol complexes and structure of the benzeneboronate ion. *J. Org. Chem.* **1959**, *24*, 769−774.
(34) Peters, J. A. Interactions between boric acid derivatives and saccharides in aqueous media: Structures and stabilities of resulting esters. *Coord. Chem. Rev.* **2014**, *268*, 1−22.
(35) Adams, J. The development of proteasome inhibitiors as anticancer drugs. *Cancer Cell* **2004**, *5*, 417−421.
(36) Antonov, V. K.; Ivanina, T. V.; Berezin, I. V.; Martinek, K. *n*-Alkylboronic acids as bifunctional reversible inhibitors of α-chymotrypsin. *FEBS Lett.* **1970**, *7*, 23−25.
(37) Lienhard, G. E.; Koehler, K. A. 2-Phenylethaneboronic acid, a possible transition-state analog for chymotrypsin. *Biochemistry* **1971**, *10*, 2477−2483.
(38) Kettner, C.; Shenvi, A. Inhibition of the serine proteases leukocyte elastase, pancreatic elastase, cathepsin G, and chymotrypsin by peptide boronic acids. *J. Biol. Chem.* **1984**, *259*, 15106−15114.
(39) Smoum, R.; Rubinstein, A.; Dembitsky, V. M.; Srebnik, M. Boron containing compounds as protease inhibitors. *Chem. Rev.* **2012**, *112*, 4156−4220.
(40) Trippier, P. C.; McGuigan, C. Boronic acids in medicinal chemistry: Anticancer, antibacterial and antiviral applications. *MedChemComm* **2010**, *1*, 183−198.
(41) Adamczyk-Woźniak, A.; Borys, K. M.; Sporzyński, A. Recent developments in the chemistry and biological applications of benzoxaboroles. *Chem. Rev.* **2015**, *115*, 5224−5247.
(42) Ellis, G. A.; Palte, M. J.; Raines, R. T. Boronate-mediate biologic delivery. *J. Am. Chem. Soc.* **2012**, *134*, 3631−3634.
(43) Ma, R.; Shi, L. Phenylboronic acid-based glucose-responsive polymeric nanoparticles: Synthesis and applications in drug delivery. *Polym. Chem.* **2014**, *5*, 1503.
(44) Wang, J.; Wu, W.; Jiang, X. Nanoscaled boron-containing delivery systems and therapeutic agents for cancer treatment. *Nanomedicine* **2015**, *10*, 1149−1163.
(45) Andersen, K. A.; Smith, T. P.; Lomax, J. E.; Raines, R. T. Boronic acid for the traceless delivery of proteins into cells. *ACS Chem. Biol.* **2016**, *11*, 319−323.
(46) Wu, X.; Li, Z.; Chen, X. X.; Fossey, J. S.; James, T. D.; Jiang, Y. B. Selective sensing of saccharides using simple boronic acids and their aggregates. *Chem. Soc. Rev.* **2013**, *42*, 8032−8048.
(47) Lippert, A. R.; Van de Bittner, G. C.; Chang, C. J. Boronate oxidation as a bioorthogonal reaction approach for studying the chemistry of hydrogen peroxide in living systems. *Acc. Chem. Res.* **2011**, *44*, 793−804.
(48) Hoang, T. T.; Smith, T. P.; Raines, R. T. A boronic acid conjugate of angiogenin that shows ROS-responsive neuroprotective activity. *Angew. Chem., Int. Ed.* **2017**, *56*, 2619−2622.
(49) Whyte, G. F.; Vilar, R.; Woscholski, R. Molecular recognition with boronic acids—applications in chemical biology. *J. Chem. Biol.* **2013**, *6*, 161−174.
(50) Cal, P. M. S. D.; Frade, R. F. M.; Cordeiro, C.; Gois, P. M. P. Reversible lysine modification on proteins using functionalized boronic acids. *Chem. - Eur. J.* **2015**, *21*, 8182−8187.
(51) Akçay, G.; Belmonte, M. A.; Aquila, B.; Chuaqui, C.; Hird, A. W.; Lamb, M. L.; Rawlins, P. B.; Su, N.; Tentarelli, S.; Grimster, N. P.; Su, Q. Inhibition of Mcl-1 through covalent modification of a noncatalytic lysine side chain. *Nat. Chem. Biol.* **2016**, *12*, 931−936.
(52) Hall, D. G. *Boronic Acids: Preparation and Applications in Organic Synthesis, Medicine and Materials*; Wiley−VCH Verlag: Weinheim, Germany, 2011.
(53) Bull, S. D.; Davidson, M. G.; van den Elsen, J. M. H.; Fossey, J. S.; Jenkins, A. T. A.; Jiang, Y.-B.; Kubo, Y.; Marken, F.; Sakurai, K.; Zhao, J.; James, T. D. Exploiting the reversible covalent bonding of boronic acids—recognition, sensing, and assembly. *Acc. Chem. Res.* **2013**, *46*, 312−326.
(54) Toxicological Profile for Boron. *U.S. Agency for Toxic Substances and Disease Registry*; U.S. Centers for Disease Control: Atlanta, GA 2016; http://www.atsdr.cdc.gov/toxprofiles/tp26-c6.pdf (accessed December 12, 2016).
(55) Baures, P. W.; Peterson, S. A.; Kelly, J. W. Discovering transthyretin amyloid fibril inhibitors by limited screening. *Bioorg. Med. Chem.* **1998**, *6*, 1389−1401.
(56) Johnson, S. M.; Connelly, S.; Wilson, I. A.; Kelly, J. W. Toward optimization of the linker substructure common to transthyretin amyloidogenesis inhibitors using biochemical and structural studies. *J. Med. Chem.* **2008**, *51*, 6348−6358.
(57) Bourgault, S.; Choi, S.; Buxbaum, J. N.; Kelly, J. W.; Price, J. L.; Reixach, N. Mechanisms of transthyretin cardiomyocyte toxicity inhibition by resveratrol analogs. *Biochem. Biophys. Res. Commun.* **2011**, *410*, 707−713.
(58) Cotrina, E. Y.; Pinto, M.; Bosch, L.; Vila, M.; Blasi, D.; Quintana, J.; Centeno, N. B.; Arsequell, G.; Planas, A.; Valencia, G. Modulation of the fibrillogenesis inhibition properties of two transthyretin ligands by halogenation. *J. Med. Chem.* **2013**, *56*, 9110−9121.
(59) Palaninathan, S. K. Nearly 200 X-ray crystal structures of transthyretin—what do they tell us about this protein and the design of drugs for TTR amyloidoses? *Curr. Med. Chem.* **2012**, *19*, 2324−2342.
(60) Muzio, T.; Cody, V.; Luft, J. R.; Pangborn, W.; Wojtczak, A. Complex of rat transthyretin with tetraiodothyroacetic acid refined at 2.1 and 1.8 Å resolution. *Acta Biochim. Polonica* **2001**, *48*, 877−884.
(61) Oza, V. B.; Smith, C.; Raman, P.; Koepf, E. K.; Lashuel, H. A.; Petrassi, H. M.; Chiang, K. P.; Powers, E. T.; Sachettinni, J. C.; Kelly, J. W. Synthesis, structure, and activity of diclofenac analogues as

DOI: 10.1021/acs.jmedchem.7b00952
J. Med. Chem. 2017, 60, 7820−7834

transthyretin amyloid fibril formation inhibitors. *J. Med. Chem.* **2002**, *45*, 321−332.
(62) Neumann, P.; Cody, V.; Wojtczak, A. Ligand binding at the transthyretin dimer−dimer interface: Structure of the transthyretin−T4Ac complex at 2.2 Å resolution. *Acta Crystallogr., Sect. D: Biol. Crystallogr.* **2005**, *61*, 1313−1319.
(63) Palaninathan, S. K.; Mohamedmohaideen, N. N.; Orlandini, E.; Ortore, G.; Nencetti, S.; Lapucci, A.; Rossello, A.; Freundlich, J. S.; Sacchettini, J. C. Novel transthyretin amyloid fibril formation inhibitors: Synthesis, biological evaluation, and X-ray structural analysis. *PLoS One* **2009**, *4*, e6290.
(64) Johnson, S. M.; Connelly, S.; Wilson, I. A.; Kelly, J. W. Biochemical and structural evaluation of highly selective 2-arylbenzoxazole-based transthyretin amyloidogenesis inhibitors. *J. Med. Chem.* **2008**, *51*, 260−270.
(65) *ChemSpider*; Society of Chemistry, London, UK, 2015; www.chemspider.com (accessed December 7, 2016).
(66) Groll, M.; Berkers, C. R.; Ploegh, H. L.; Ovaa, H. Crystal structure of the boronic acid-based proteasome inhibitor bortezomib in complex with the yeast 20S proteasome. *Structure* **2006**, *14*, 451−456.
(67) Bone, R.; Frank, D.; Kettner, C. A.; Agard, D. A. Structural analysis of specificity: α-Lytic protease complexes with analogues of reaction intermediates. *Biochemistry* **1989**, *28*, 7600−7609.
(68) Eriksson, A. E.; Baase, W. A.; Zhang, X.-J.; Heinz, D. W.; Blaber, M.; Baldwin, E. P.; Matthews, B. W. Response of a protein structure to cavity-creating mutations and its relation to the hydrophobic effect. *Science* **1992**, *255*, 178−183.
(69) Kawasaki, Y.; Chufan, E. E.; Lafont, V.; Hidaka, K.; Kiso, Y.; Mario Amzel, L.; Freire, E. How much binding affinity can be gained by filling a cavity? *Chem. Biol. Drug Des.* **2010**, *75*, 143−151.
(70) Voth, A. R.; Khuu, P.; Oishi, K.; Ho, P. S. Halogen bonds as orthogonal molecular interactions to hydrogen bonds. *Nat. Chem.* **2009**, *1*, 74−79.
(71) Riley, K. E.; Merz, K. M., Jr. Insights into the strength and origin of halogen bonding: The halobenzene-formaldehyde dimer. *J. Phys. Chem. A* **2007**, *111*, 1688−1694.
(72) Yamamoto, Y.; Matsumura, T.; Takao, N.; Yamagishi, H.; Takahashi, M.; Iwatsuki, S.; Ishihara, K. Fast trigonal/tetragonal interconversion followed by slow chelate-ring closure in the complexation of boronic acids. *Inorg. Chim. Acta* **2005**, *358*, 3355−3361.
(73) Peters, J. A. Interactions between boric acid derivatives and saccharides in aqueous media: Structures and stabilities of resulting esters. *Coord. Chem. Rev.* **2014**, *268*, 1−22.
(74) Alhamadsheh, M. M.; Connelly, S.; Cho, A.; Reixach, N.; Powers, E. T.; Pan, D. W.; Wilson, I. A.; Kelly, J. W.; Graef, I. A. Potent kinetic stabilizers that prevent transthyretin-mediated cardiomyocyte proteotoxicity. *Sci. Transl. Med.* **2011**, *3*, 97ra81.
(75) Zhu, C.; Wang, R.; Falck, J. R. Mild and rapid hydroxylation of aryl/heteroaryl boronic acids and boronate esters with *N*-oxides. *Org. Lett.* **2012**, *14*, 3494−3497.
(76) Windsor, I. W.; Raines, R. T. Fluorogenic assay for inhibitors of HIV-1 protease with sub-picomolar affinity. *Sci. Rep.* **2015**, *5*, 11286.
(77) McCutchen, S. L.; Colon, W.; Kelly, J. W. Transthyretin mutation Leu-55-Pro significantly alters tetramer stability and increases amyloidogenicity. *Biochemistry* **1993**, *32*, 12119−12127.
(78) Grimm, F. A.; Lehmler, H. J.; He, X.; Robertson, L. W.; Duffel, M. W. Sulfated metabolites of polychlorinated biphenyls are high-affinity ligands for the thyroid hormone transport protein transthyretin. *Environ. Health Perspect.* **2013**, *121*, 657−662.
(79) Giraldo, J.; Vivas, N. M.; Vila, E.; Badia, A. Assessing the (a)symmetry of concentration-effect curves: Empirical versus mechanistic models. *Pharmacol. Ther.* **2002**, *95*, 21−45.
(80) Miroy, G. J.; Lai, Z.; Lashuel, H. A.; Peterson, S. A.; Strang, C.; Kelly, J. W. Inhibiting transthyretin amyloid fibril formation via protein stabilization. *Proc. Natl. Acad. Sci. U. S. A.* **1996**, *93*, 15051−15056.
(81) Otwinowski, Z.; Minor, W. Processing of X-ray diffraction data collected in oscillation mode. *Methods Enzymol.* **1997**, *276*, 307−326.
(82) Adams, P. D.; Afonine, P. V.; Bunkoczi, G.; Chen, V. B.; Davis, I. W.; Echols, N.; Headd, J. J.; Hung, L. W.; Kapral, G. J.; Grosse-Kunstleve, R. W.; McCoy, A. J.; Moriarty, N. W.; Oeffner, R.; Read, R. J.; Richardson, D. C.; Richardson, J. S.; Terwilliger, T. C.; Zwart, P. H. PHENIX: A comprehensive Python-based system for macromolecular structure solution. *Acta Crystallogr., Sect. D: Biol. Crystallogr.* **2010**, *66*, 213−221.
(83) Emsley, P.; Lohkamp, B.; Scott, W. G.; Cowtan, K. Features and development of Coot. *Acta Crystallogr., Sect. D: Biol. Crystallogr.* **2010**, *66*, 486−501.

DOI: 10.1021/acs.jmedchem.7b00952
J. Med. Chem. 2017, 60, 7820−7834